Journal of Food and Drug Analysis

Volume 29 | Issue 3 Article 5

2021

Mesonosides A-H, primeverose derivatives from Mesona procumbens suppress adipogenesis by downregulating PPARg and C/EBPa in 3T3-L1 cells

Recommended Citation

Huang, Hung-Tse; Liaw, Chia-Ching; Chiou, Chun-Tang; Lee, Kung-Ta; and Kuo, Yao-Haur (2021) "Mesonosides A-H, primeverose derivatives from Mesona procumbens suppress adipogenesis by downregulating PPARg and C/EBPa in 3T3-L1 cells," *Journal of Food and Drug Analysis*: Vol. 29 : Iss. 3 , Article 5.
Available at: https://doi.org/10.38212/2224-6614.3365

ORIGINAL ARTICLE

Mesonosides A-H, primeverose derivatives from *Mesona procumbens* suppress adipogenesis by downregulating PPARγ and C/EBPα in 3T3-L1 cells

Hung-Tse Huang [a,b], Chia-Ching Liaw [b,c], Chun-Tang Chiou [b], Kung-Ta Lee [a,**], Yao-Haur Kuo [b,d,*]

[a] Department of Biochemical Science and Technology, National Taiwan University, Taipei, 10617, Taiwan
[b] Division of Chinese Materia Medica Development, National Research Institute of Chinese Medicine, Taipei, 11221, Taiwan
[c] Department of Biochemical Science and Technology, National Chiayi University, Chiayi, 60004, Taiwan
[d] Graduate Institute of Integrated Medicine, College of Chinese Medicine, China Medical University, Taichung, 40447, Taiwan

Abstract

Obesity is becoming a worldwide epidemic, especially in industrialized countries. We hereby report a methanolic extract of *Mesona procumbens* (known as Hsian-tsao in Taiwan) significantly inhibits lipid accumulation in 3T3-L1 adipocytes, and eight new primeverose derivatives, mesonosides A-H (1−8), were isolated from the methanolic extract of *M. procumbens*. Structural elucidation of 1−8 was established by spectroscopic methods, especially 2D NMR techniques (^{1}H−^{1}H COSY, HSQC, HMBC, and NOESY) and HRESIMS. Anti-obesity evaluation revealed that isolates 1−5, 7, and 8 showed inhibitory effects on lipid accumulation and protein levels of adipogenic transcription factor, PPARγ and C/EBPα in 3T3-L1 cells. Our study suggests that *M. procumbens* extract including new primeverose isolates may be potentially used as a natural source to ameliorate fat accumulation and even obesity.

Keywords: Anti-adipogenic, Lipid accumulation, *Mesona procumbens*, Mesonoside, PPARγ

1. Introduction

Obesity has become the leading metabolic disease globally [1] and has been associated with other diseases, such as coronary heart disease, hypertension, type 2 diabetes mellitus, cancer, respiratory complications, and osteoarthritis [2]. Obesity is a condition in which adipocytes accumulate a large amount of fat and become enlarged. At the cellular level, obesity is characterized by an increase in the number and size of adipocytes differentiated from fibroblastic preadipocytes in adipose tissue [3]. Adipocyte differentiation is a complex process involving changes in cell morphology, hormone sensitivity, and gene expression [4]. The transcription factors CCAAT/enhancer binding protein (C/EBP) β and δ are first induced in response to adipogenic factors and then in turn activate peroxisome proliferator-activated receptor gamma (PPARγ) and C/EBPα [5], which are essential for the expression of a large group of genes that produce the adipocyte phenotype [6]. An increasing number of investigations have been conducted to discover the components that may reduce the accumulation of excess body fat. More recently, eugenol diglycosides have been reported to inhibit lipid droplet accumulation in adipocytes by reducing the transcription levels of adipocyte marker genes [7].

Received 23 February 2021; revised 16 April 2021; accepted 31 May 2021.
Available online 15 September 2021.

* Corresponding author at: Division of Chinese Materia Medica Development, National Research Institute of Chinese Medicine, Taipei, 11221, Taiwan. Fax: +886 2 28236150.
** Corresponding author at: Department of Biochemical Science and Technology, National Taiwan University, Taipei, 10617, Taiwan. Fax: +886 2 23640961.
E-mail addresses: ktlee@ntu.edu.tw (K-T. Lee), kuoyh@nricm.edu.tw (Y-H. Kuo).

https://doi.org/10.38212/2224-6614.3365

Mesona procumbens Hemsl., known as Hsian-tsao in Taiwan, is a common material used to prepare functional beverages in several Asia countries and is also frequently used as an ingredient in traditional Chinese medicine to treat heat shock, hypertension, diabetes, liver disease, and muscle pain [8]. Previous research reported that *M. procumbens* extracts possess several bioactivities, such as anti-inflammatory [9], antihypertensive [10], DNA damage protection [11], antimutagenic [12], liver fibrosis prevention [13], and renal protective [14] activities. However, the active components in *M. procumbens* extracts imparting these effects are not well defined.

Since obesity increases the risk of several metabolic diseases, the effective components for ameliorating excess body fat accumulation are worth investigating. To our knowledge, there is no report about the effect of *M. procumbens* on the regulation of adipogenesis or obesity. In the present study, we demonstrated that the methanolic extract of *M. procumbens* exhibited significant anti-adipogenesis activity. Here, 3T3-L1 cells were used as a cell model for adipose cell biology research, which has been well established over the course of several decades [15,16].

2. Materials and methods

2.1. General experimental procedures

Optical rotations were determined by using a P-2000 polarimeter (JASCO). Infrared (IR) spectra were recorded on a Mattson Genesis II spectrometer (Thermo). High-resolution electrospray ionization mass spectrometry (HRESIMS) data were obtained on an LCQ mass spectrometer (Thermo). High-resolution electrospray ionization mass spectrometry (HRESIMS) data were measured on a Shimadzu IT-TOF HR mass spectrometer. Nuclear magnetic resonance (NMR) spectra were recorded on Varian Unity Inova 500 MHz, or Varian VNMRS 600 MHz spectrometers. For column chromatography (CC), and silica gel 60 (70−230 and 230−400 mesh, Merck) were used. Precoated silica gel plates (Merck 60 F-254) were used for thin layer chromatography (TLC). High-performance liquid chromatography (HPLC) separations were performed on a Shimadzu LC-8A pump with a UV SPD-20A detector equipped with a 250 × 20 mm i.d. preparative Cosmosil $5C_{18}$ AR-II column (Nacalai Tesque).

2.2. Plant material

The whole plants of *M. procumbens* Hemsl. (8.0 kg, dry weight) were purchased from Starsci Biotech Co. Ltd. in Taoyuan and identified by Dr. Syh-Yuan Hwang of the Endemic Species Research Institute, Council of Agriculture, Taiwan. A voucher specimen (No. NRICM20190901) was deposited in the National Research Institute of Chinese Medicine, Ministry of Health and Welfare, Taipei, Taiwan.

2.3. Extraction and isolation

Air-dried *M. procumbens* (8.0 kg) were extracted with 100% methanol (80 L) at 50 °C three times, and the extract was concentrated under reduced pressure. The methanol extract (*ca.* 796.5 g, MPM) was suspended in H_2O, and the suspension was partitioned successively with *n*-hexane and then CH_2Cl_2, respectively. The partition layers were concentrated under reduced pressure to obtain hexane (MPH) and CH_2Cl_2 (MPD) extracts. The MPD extract (*ca.* 47.6 g) was separated into 6 fractions (Fractions I~VI) on a C_{18} gel flash column (60−230 mesh, 15 × 25 cm) eluting with a solvent system of H_2O/MeOH (0−100%). Fraction IV was further subjected to a silica gel flash column (60−230 mesh, 15 × 20 cm) eluting with a solvent system of CH_2Cl_2/acetone (5−100%) to afford eight subfractions (IVA~IVH). The IVF fraction was fractionated by preparative HPLC eluting with 60% acetonitrile (ACN) in H_2O (flow rate: 10.0 mL/min) to give 7 fractions (IVF-1~IVF-7). Fraction IVF-3 was separated by HPLC eluting with 45% ACN (flow rate: 10.0 mL/min) to give compound **1** (102.3 mg, Rt: 19.8 min). Fraction IVE was separated by HPLC with 60% ACN (flow rate: 10.0 mL/min) to afford nine fractions (IVE-1~IVE-9). IVE-4 was purified by preparative HPLC eluting with 50% ACN (flow rate: 10.0 mL/min) to give **2** (76.6 mg, Rt: 19.3 min) and **3** (34.3 mg, Rt: 22.3 min). Fraction IVD was separated by HPLC with 65% ACN (flow rate: 10.0 mL/min) to afford seven fractions (IVD-1~IVD-7). The IVD-4 fraction was further purified by HPLC, repeatedly eluting with 50% ACN (flow rate: 10.0 mL/min), to give **4** (39.6 mg, Rt: 22.8 min). Compound **5** (4.6 mg, Rt: 25.1 min) was purified from fraction IVD-5 by HPLC eluting with 50% ACN (flow rate: 10.0 mL/min). Fraction IVC was separated by HPLC with 65% ACN (flow rate: 10.0 mL/min) to afford eight fractions (IVC-1~IVD-8). The IVC-7 fraction was further purified by HPLC and repeatedly eluted with 45% ACN (flow rate: 10.0 mL/min) to give **6** (0.9 mg, Rt: 82.3 min). Fraction IVB was separated by HPLC with 65% ACN (flow rate: 10.0 mL/min) elution to afford six fractions (IVB-1~IVB-6). The IVB-4 fraction was further purified by HPLC with repeated elution with 50% ACN (flow rate: 10.0 mL/min) to give **7** (23.1 mg, Rt: 38.4 min) and **8** (9.1 mg, Rt: 44.0 min).

*Table 1. ^{1}H-NMR spectroscopic data (methanol-d_4) for compounds **1**–**8**.*

NO	1[a]	2[a]	3[a]	4[a]	5[a]	6[b]	7[b]	8[a]
1	4.57 d (7.5)	4.54 d (8.0)	4.48 d (8.0)	4.57 d (8.0)	4.57 d (8.0)	4.76 d (7.8)	4.51 d (7.8)	4.55 d (8.0)
2	3.61 dd (8.0, 9.5)	3.58 m	3.49 dd (8.0, 9.5)	3.60 dd (8.0, 9.5)	3.61 dd (8.0, 9.5)	5.03 dd (8.4, 10.2)	3.55 dd (8.4, 9.6)	3.59 m
3	5.36 t (9.5)	5.34 t (9.0)	5.19 m	5.36 t (9.5)	5.36 t (9.5)	5.46 t (9.6)	5.30 t (9.6)	5.34 t (9.5)
4	5.12 dd (9.5, 10.0)	5.04 t (9.5)	3.53 m	5.11 t (10.0)	5.11 t (10.0)	5.09 t (9.6)	5.01 t (9.6)	5.05 dd (9.0, 9.5)
5	3.83 m	3.73 m	3.51 m	3.84 m	3.84 m	3.79 m	3.71 m	3.76 m
6	3.20 dd (10.0, 11.0) 3.87 m	3.58 m 3.86 dd (2.0, 11.0)	3.75 m 4.07 dd (1.5, 11.5)	3.69 dd (5.5, 11.5) 3.88 dd (2.0, 11.5)	3.67 dd (5.5, 11.5) 3.87 dd (2.0, 11.0)	3.57 dd (5.4, 11.4) 3.84 dd (2.4, 11.4)	3.59 dd (5.4, 11.4) 3.83 dd (2.4, 11.4)	3.59 m 3.87 dd (2.5, 11.0)
1′	4.31 d (7.5)	4.46 d (8.0)	4.72 d (8.0)	4.43 d (7.5)	4.35 d (7.0)	4.41 d (7.8)	4.58 d (7.8)	4.52 d (8.0)
2′	3.22 t (7.5)	4.71 dd (8.0, 9.5)	4.79 dd (8.0, 9.5)	3.34 dd (7.0, 9.0)	3.30 dd (7.5, 9.0)	4.68 dd (7.8, 9.6)	4.74 dd (7.2, 9.0)	4.79 m
3′	3.33 m	3.45 t (9.0)	5.00 t (9.5)	4.89 t (9.0)	3.57 t (9.0)	3.42 t (9.6)	4.95 t (9.6)	3.72 t (8.0)
4′	3.50 ddd (5.0, 8.5, 13.5)	3.57 m	3.74 m	3.64 m	4.71 ddd (5.5, 9.0, 10.0)	3.54 ddd (5.4, 8.4, 13.8)	3.70 m	4.78 m
5′	3.66 dd (5.5, 11.5) 3.87 m	3.22 dd (10.0, 11.5) 3.91 dd (5.5, 11.5)	3.32 m 3.97 dd (5.5, 11.5)	3.29 dd (10.0, 11.5) 3.93 dd (5.0, 11.5)	3.25 dd (10.0, 11.5) 3.98 dd (5.5, 11.5)	3.19 dd (10.2, 11.4) 3.88 dd (5.4, 11.4)	3.28 m 3.94 dd (5.4, 12.0)	3.30 dd (9.5, 11.5) 4.04 dd (5.0, 11.5)
1″	5.16 ddd (1.0, 1.5, 10.5) 5.29 ddd (1.0, 1.5, 17.0)	5.17 ddd (1.0, 1.5, 17.0) 5.29 ddd (1.0, 1.5, 17.0)	5.31 ddd (1.5, 2.0, 17.0) 5.19 m	5.17 ddd (1.5, 2.0, 17.5) 5.31 ddd (1.5, 2.0, 10.5)	5.16 ddd (1.0, 1.5, 10.5) 5.29 ddd (1.0, 1.5, 17.0)	5.12 ddd (1.0, 1.5, 17.4) 5.24 ddd (1.0, 1.5, 10.8)	5.14 ddd (1.2, 2.4, 10.8) 5.27 ddd (1.2, 2.4, 16.8)	5.17 ddd (1.0, 1.5, 10.5) 5.29 ddd (1.0, 1.5, 17.0)
2″	5.92 ddd (7.0, 10.5, 17.5)	5.91 ddd (6.5, 10.5, 17.0)	5.94 ddd (6.5, 10.5, 17.0)	5.39 ddd (7.0, 10.5, 17.5)	5.92 ddd (7.0, 10.5, 17.0)	5.85 ddd (6.6, 10.8, 17.4)	5.89 ddd (7.2, 10.8, 16.8)	5.91 ddd (7.0, 10.5, 17.0)
3″	4.22 ddd (6.0, 6.0, 12.0)	4.18 ddd (6.0, 6.0, 12.0)	4.20 ddd (6.5, 6.5, 13.0)	4.23 ddd (6.5, 6.5, 13.0)	4.22 ddd (6.5, 6.5, 13.0)	4.10 ddd (6.0, 6.0, 12.0)	4.15 ddd (6.0, 6.0, 12.0)	4.18 ddd (6.0, 6.0, 12.0)
4″	1.56 m 1.70 m	1.57 m 1.71 m	1.58 m 1.70 m	1.57 m 1.69 m	1.57 m 1.70 m	1.50 m 1.56 m	1.54 m 1.67 m	1.58 m 1.71 m
5″	1.42 m	1.42 m	1.42 m	1.42 m	1.42 m	1.28 m	1.39 m	1.43 m
6″	1.33 m	1.33 m	1.33 m	1.32 m	1.33 m	1.28 m	1.30 m	1.34 m
7″	1.34 m	1.34 m	1.35 m	1.34 m	1.34 m	1.29 m	1.31 m	1.35 m
8″	0.92 t (7.0)	0.93 t (7.0)	0.93 t (7.0)	0.92 t (6.5)	0.93 t (7.0)	0.89 t (6.6)	0.89 t (6.6)	0.93 t (7.0)
3‴	8.02 m	8.02 m	8.09 m	8.02 m	8.02 m	7.92 m	7.98 m	8.02 m
4‴	7.49 m	7.49 m	7.50 m	7.49 m	7.49 m	7.45 m	7.45 m	7.49 m
5‴	7.63 m	7.63 m	7.63 m	7.63 m	7.63 m	7.60 m	7.59 m	7.63 m
6‴	7.49 m	7.49 m	7.50 m	7.49 m	7.49 m	7.45 m	7.45 m	7.49 m
7‴	8.02 m	8.02 m	8.09 m	8.02 m	8.02 m	7.92 m	7.98 m	8.02 m
2-OAc						1.91 s		
4-OAc	1.92 s	1.91 s		1.92 s	1.92 s	1.90 s	1.87 s	1.92 s
2′-OAc		2.15 s	2.07 s			2.12 s	2.03 s	2.15 s
3′-OAc			2.06 s	2.14 s			2.04 s	
4′-OAc					2.09 s			2.01 s

[a] Recorded at 500 MHz.
[b] Record at 600 MHz.

*Table 2. ^{13}C-NMR Spectroscopic Data (methanol-d_4) for compounds **1**–**8**.*

NO	1[a]	2[a]	3[a]	4[a]	5[a]	6[b]	7[b]	8[a]
1	101.9, CH	101.8, CH	102.0, CH	101.9, CH	101.9, CH	99.5, CH	101.9, CH	101.8, CH
2	72.1, CH	72.0, CH	72.2, CH	72.1, CH	72.1, CH	71.7, CH	72.0, CH	72.0, CH
3	75.9, CH	75.9, CH	78.3, CH	75.9, CH	75.8, CH	73.9, CH	75.9, CH	75.9, CH
4	69.3, CH	69.2, CH	68.6, CH	69.3, CH	69.4, CH	68.9, CH	69.0, CH	69.2, CH
5	72.9, CH	72.8, CH	75.9, CH	73.0, CH	72.9, CH	72.8, CH	72.9, CH	72.7, CH
6	67.5, CH_2	67.0, CH_2	68.0, CH_2	67.5, CH_2	67.6, CH_2	66.8, CH_2	67.0, CH_2	67.1, CH_2
1′	103.8, CH	101.4, CH	101.3, CH	103.5, CH	103.7, CH	101.3, CH	100.8, CH	101.1, CH
2′	73.4, CH	73.6, CH	71.9, CH	71.4, CH	73.5, CH	73.6, CH	71.6, CH	73.2, CH
3′	76.1, CH	74.7, CH	75.3, CH	76.9, CH	73.3, CH	74.6, CH	75.3, CH	71.4, CH
4′	69.8, CH	69.8, CH	67.8, CH	68.0, CH	71.7, CH	69.7, CH	67.7, CH	71.4, CH
5′	65.5, CH_2	65.6, CH_2	65.3, CH_2	65.2, CH_2	62.2, CH_2	65.5, CH_2	65.2, CH_2	62.0, CH_2
1″	115.0, CH	114.9, CH	114.8, CH	114.9, CH	115.0, CH	114.9, CH	114.8, CH	115.0, CH
2″	139.3, CH	139.3, CH	139.4, CH	139.3, CH	139.3, CH	138.9, CH	139.3, CH	139.3, CH
3″	81.7, CH	81.6, CH	81.4, CH	81.7, CH	81.7, CH	81.9, CH	81.7, CH	81.7, CH
4″	34.4, CH_2	34.4, CH_2	34.5, CH_2	34.5, CH_2	34.4, CH_2	34.5, CH_2	34.4, CH_2	34.4, CH_2
5″	24.2, CH_2	24.2, CH_2	24.3, CH_2	24.3, CH_2	24.2, CH_2	24.2, CH_2	24.2, CH_2	24.2, CH_2
6″	31.6, CH_2	31.6, CH_2	31.7, CH_2	31.6, CH_2	31.6, CH_2	31.5, CH_2	31.6, CH_2	31.6, CH_2
7″	22.3, CH_2	22.3, CH_2	22.2, CH_2	22.3, CH_2	22.3, CH_2	22.3, CH_2	22.2, CH_2	22.3, CH_2
8″	13.0, CH_3	13.0, CH_3	13.0, CH_3	13.0, CH_3	13.0, CH_3	12.9, CH_3	12.9, CH_3	13.0, CH_3
1‴	166.1, qC	166.1, qC	166.5, qC	166.1, qC	166.1, qC	165.7, qC	166.1, qC	166.1, qC
2‴	129.7, CH	129.1, CH	130.3, CH	129.7, CH	129.7, CH	129.0, CH	129.7, CH	129.8, CH
3‴	128.2, CH	128.1, CH	128.1, CH	129.3, CH	129.3, CH	129.3, CH	129.3, CH	129.3, CH
4‴	129.3, CH	129.3, CH	129.3, CH	128.2, CH	128.2, CH	128.2, CH	128.1, CH	128.1, CH
5‴	133.0, CH	133.0, CH	132.8, CH	133.0, CH	133.0, CH	133.3, CH	133.0, CH	133.0, CH
6‴	129.3, CH	129.3, CH	129.3, CH	128.2, CH	128.2, CH	128.2, CH	128.1, CH	128.1, CH
7‴	128.2, CH	128.1, CH	128.1, CH	129.3, CH	129.3, CH	129.3, CH	129.3, CH	129.3, CH
2-OAc						169.5, qC 19.2, CH_3		
4-OAc	170.3, qC 19.2, CH_3	169.9, qC 19.2, CH_3		170.2, qC 19.3, CH_3	170.2, qC 19.2, CH_3	169.7, qC 19.1, CH_3	169.8, qC 19.1, CH_3	169.9, qC 19.2, CH_3
2′-OAc		170.6, qC 19.9, CH_3	167.0, qC 19.6, CH_3			170.6, qC 19.8, CH_3	170.1, qC 19.4, CH_3	170.4, qC 19.3, CH_3
3′-OAc			170.7, qC 19.4, CH_3	171.2, qC 19.7, CH_3			170.7, qC 19.5, CH_3	
4′-OAc					170.8, qC 19.4, CH_3			170.6, qC 19.8, CH_3

[a] Recorded at 125 MHz.
[b] Recorded at 150 MHz.

2.3.1. Mesonoside A (1)

Colorless syrup; $[\alpha]_D^{25}$ -0.45 (*c* 0.6, MeOH); UV λ_{max} (MeOH) (log ϵ) 273 (2.96), 229 (4.13) nm; IR (KBr) ν_{max} 3414, 2932, 2865, 1731, 1274, 1047 cm^{-1}; ^{1}H and ^{13}C-NMR spectroscopic data (methanol-d_4) are shown in Tables 1 and 2, respectively; HRESIMS *m/z* 591.2419 $[M + Na]^+$ (calcd. for $C_{28}H_{40}O_{12}Na$, 591.2412).

2.3.2. Mesonoside B (2)

Colorless syrup; $[\alpha]_D^{25}$ -0.72 (*c* 0.6, MeOH); UV λ_{max} (MeOH) (log ϵ) 273 (3.01), 229 (4.06) nm; IR (KBr) ν_{max} 3419, 2932, 2860, 1734, 1277, 1039 cm^{-1}; ^{1}H and ^{13}C-NMR spectroscopic data (methanol-d_4) are shown in Tables 1 and 2, respectively; HRESIMS *m/z* 633.2504 $[M + Na]^+$ (calcd. for $C_{30}H_{42}O_{13}Na$, 633.2518).

2.3.3. Mesonoside C (3)

Colorless syrup; $[\alpha]_D^{25}$ -3.24 (*c* 0.6, MeOH); UV λ_{max} (MeOH) (log ϵ) 273 (3.10), 229 (4.04) nm; IR (KBr) ν_{max} 3441, 2930, 2864, 1726, 1247, 1042 cm^{-1}; ^{1}H and ^{13}C-NMR spectroscopic data (methanol-d_4) are shown in Tables 1 and 2, respectively; HRESIMS *m/z* 633.2501 $[M + Na]^+$ (calcd. for $C_{30}H_{42}O_{13}Na$, 633.2518).

2.3.4. Mesonoside D (4)

Colorless syrup; $[\alpha]_D^{25}$ -0.68 (*c* 0.6, MeOH); UV λ_{max} (MeOH) (log ϵ) 273 (3.04), 229 (4.00) nm; IR (KBr) ν_{max} 3456, 2932, 2863, 1729, 1277, 1039 cm^{-1}; ^{1}H and ^{13}C-NMR spectroscopic data (methanol-d_4) are shown in Tables 1 and 2, respectively; HRESIMS *m/z* 633.2500 $[M + Na]^+$ (calcd. for $C_{30}H_{42}O_{13}Na$, 633.2518).

2.3.5. Mesonoside E (5)

Colorless syrup; $[\alpha]_D^{25}$ -6.56 (*c* 0.6, MeOH); UV λ_{max} (MeOH) (log ϵ) 273 (3.07), 229 (4.07) nm; IR (KBr) ν_{max} 3468, 2932, 2858, 1741, 1274, 1037 cm^{-1}; ^1H and ^{13}C-NMR spectroscopic data (methanol-d_4) are shown in Tables 1 and 2, respectively; HRESIMS *m/z* 633.2507 $[M + Na]^+$ (calcd. for $C_{30}H_{42}O_{13}Na$, 633.2518).

2.3.6. Mesonoside F (6)

Colorless syrup; $[\alpha]_D^{25}$ -0.85 (*c* 0.6, MeOH); UV λ_{max} (MeOH) (log ϵ) 273 (3.01), 229 (4.06) nm; IR (KBr) ν_{max} 3421, 2932, 2858, 1734, 1274, 1042 cm^{-1}; ^1H and ^{13}C-NMR spectroscopic data (methanol-d_4) are shown in Tables 1 and 2, respectively; HRESIMS *m/z* 675.2639 $[M + Na]^+$ (calcd. for $C_{32}H_{44}O_{14}Na$, 675.2623).

2.3.7. Mesonoside G (7)

Colorless syrup; $[\alpha]_D^{25}$ -0.54 (*c* 0.6, MeOH); UV λ_{max} (MeOH) (log ϵ) 273 (2.93), 229 (3.94) nm; IR (KBr) ν_{max} 3473, 2935, 2860, 1756, 1245, 1035 cm^{-1}; ^1H and ^{13}C-NMR spectroscopic data (methanol-d_4) are shown in Tables 1 and 2, respectively; HRESIMS *m/z* 675.2631 $[M + Na]^+$ (calcd. for $C_{32}H_{44}O_{14}Na$, 675.2623).

2.3.8. Mesonoside H (8)

Colorless syrup; $[\alpha]_D^{25}$ -0.38 (*c* 0.6, MeOH); UV λ_{max} (MeOH) (log ϵ) 273 (3.04), 229 (4.04) nm; IR (KBr) ν_{max} 3434, 2932, 2860, 1729, 1252, 1042 cm^{-1}; ^1H and ^{13}C-NMR spectroscopic data (methanol-d_4) are shown in Tables 1 and 2, respectively; HRESIMS *m/z* 675.2603 $[M + Na]^+$ (calcd. for $C_{32}H_{44}O_{14}Na$, 675.2623).

2.4. Acid hydrolysis of glycosides

Each isolated compound (1.0 mg) was treated with 2 N methanolic HCl (2 mL) under reflux at 90 °C for 1 h. Each mixture was extracted with CH_2Cl_2 to afford the aglycone portion, and the aqueous layer was neutralized with Na_2CO_3 and filtered. Chlorotrimethylsilane and triethylamine in *N,N*-dimethylformamide (3 mL each) were added to the evaporated filtrate, and the mixture was stirred at 30 °C for 12 h. After the reaction mixture was dried under a stream of N_2, each residue was partitioned between *n*-hexane and H_2O. Each *n*-hexane fraction was subjected to gas chromatography (GC, column: Agilent Technologies capillary column DB-5MS for optical isomers, 30 m × 0.25 mm, 0.25 μm; column temperature: 130–155 °C, 2 °C/min; 155–165 °C, 0.9 °C/min; 165–195 °C, 10.0 °C/min; and 195–250 °C, 30.0 °C/min; injector temperature, 250 °C; He carrier gas, 2.0 kg/cm^3; mass detector, Thermo, DSQ2; electron energy, 70 eV). Under these conditions, the sugars of each reactant were identified by comparison with authentic D-glucose (t_R = 26.35 min) and D-xlyose (t_R = 17.23 min) standards.

2.5. Cell culture, treatments, and cell viability assay

3T3-L1 preadipocytes (BCRC Number: 60159) were plated into 6-well plates and maintained in DMEM supplemented with 10% bovine calf serum at 37 °C in a humidified 5% CO_2 incubator. Adipocytic differentiation was induced by differentiation medium A, which was added to the culture medium every 48 h for 4 d. Afterwards, the medium was changed to differentiation medium B and was freshly replaced every day [14]. The cells were harvested 8 d after the initiation of differentiation. Cell proliferation was evaluated using Cell Counting Kit-8 (CCK-8; Dojindo, Rockville, MD, USA) according to the manufacturer's instructions. All experiments were performed in triplicates.

2.6. Oil Red O staining of 3T3-L1 adipocytes

Intracellular lipid accumulation was measured using Oil red O. Fresh Oil red O solution (0.5% in isopropanol, 60 mL) and 40 mL of deionized water were prepared for the Oil red O working solution. Cells were incubated with test samples for 72 h at 37 °C in a humidified 5% CO_2 incubator. Cells were washed twice with PBS pH 7.4 and then fixed with 10% neutral buffered formalin for at least 20 min at room temperature. After fixation, the cells were washed twice with PBS and stained with Oil red O working solution for 60 min. Images of stained cells were photographed and then eluted with stained Oil red O by adding 100% isopropanol. The optical density (OD) was measured at 510 nm in a spectrophotometer (Thermo Multiskan Spectrum).

2.7. Western blot assay

Cells were lysed in RIPA buffer with phenylmethylsulfonyl fluoride (PMSF; Beyotime Biotechnology, Jiangsu, China). Protein concentration was determined using a Bio-Rad protein assay system (Bio-Rad, Hercules, CA, USA). Equivalent amounts of proteins were separated by SDS–PAGE and then transferred to PVDF membranes (Bio-Rad). After being blocked in TBS containing 5% nonfat milk, the

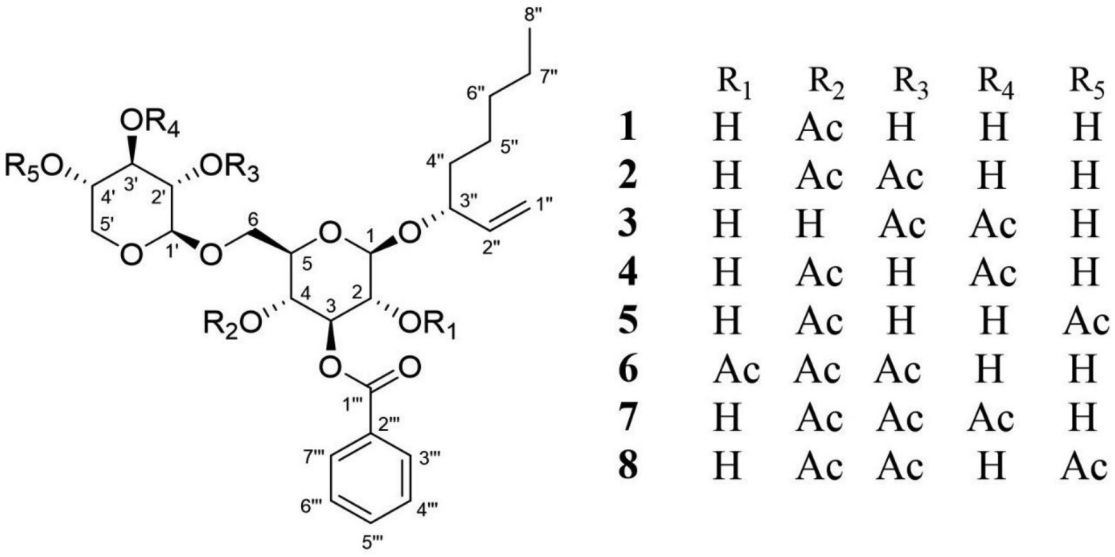

	R_1	R_2	R_3	R_4	R_5
1	H	Ac	H	H	H
2	H	Ac	Ac	H	H
3	H	H	Ac	Ac	H
4	H	Ac	H	Ac	H
5	H	Ac	H	H	Ac
6	Ac	Ac	Ac	H	H
7	H	Ac	Ac	Ac	H
8	H	Ac	Ac	H	Ac

*Fig. 1. Chemical structure of compounds **1**−**8** isolated from M. procumbens.*

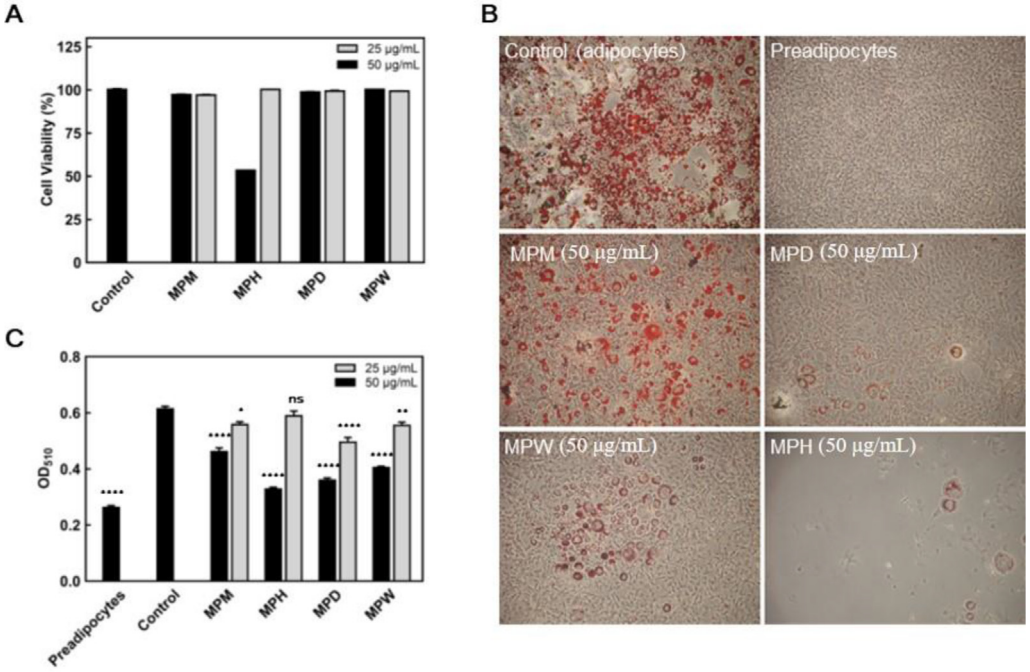

*Fig. 2. Effects of M. procumbens extracts on the cytotoxicity and adipogenesis of 3T3-L1 cells. (A) Cell viability of the MPM, MPH, MPD, and MPW fractions. Lipid accumulation was visualized (B) and quantified (C) by Oil Red O staining. Cells were photographed at 100 × magnification, and morphological changes were assessed based on lipid accumulation with or without the extracts (25 and 50 μg/mL) on d 8. The OD value of each sample at 510 nm was measured using an ELISA reader. Values are presented as the mean ± SD (n = 3). The values with different letters indicate significant differences as determined by Dunnett's method. *p < 0.05, **p < 0.01, ***p < 0.001, ****p < 0.0001 relative to the control group.*

membranes were incubated with primary antibodies (1:1000 dilution) at 4 °C for 12 h and then with horseradish peroxidase-conjugated secondary antibody (1:5000 dilution). Signals were detected on X-ray film using an ECL detection system (Pierce, Rockford, IL, USA). The relative protein levels were calculated based on β-actin as the loading control.

2.8. Statistical analysis

The results of this investigation are the means ± SD of three independent experiments. One-way ANOVA followed by Dunnett's *t*-test was used to analyze the differences between samples at different doses. The statistical analysis was performed with GraphPad Prism 7.0 software (GraphPad, La Jolla, CA). $*p < 0.05$, $**p < 0.01$, $***p < 0.001$, $****p < 0.0001$ relative to the control-treated group.

3. Results and discussion

3.1. Extraction, fractionation, and purification of the extract from M. procumbens

The methanolic extract of the whole *M. procumbens* plant (MPM, 796.5 g/8 kg, 9.95%) was suspended in H_2O and partitioned with *n*-hexane and then CH_2Cl_2 successively to yield two organic layers (MPH and MPD) and one H_2O layer (MPW). The CH_2Cl_2 extract (MPD, 5.98%) was chromatographically separated on a C_{18} gel flash column followed by a silica gel flash column. The highest-yielding fractions were further subjected to preparative HPLC using a reversed-phase (ODS) column to yield eight new primeverose derivatives, mesonosides A-H (Fig. 1). These structures were determined by spectroscopic data, especially NMR and HRMS data. All isolated compounds **1**–**8** were screened for anti-adipogenesis activity and further demonstrated the relationship of adipogenesis protein expression.

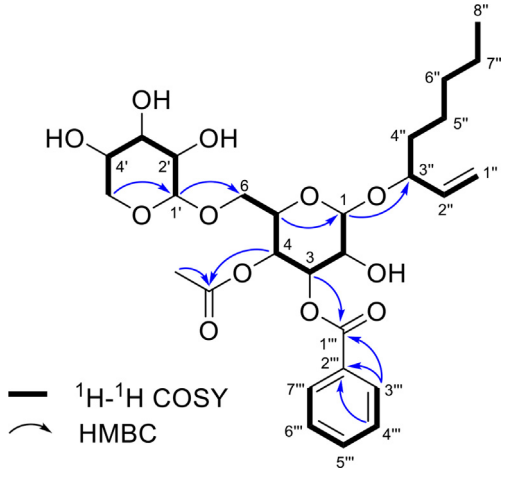

*Fig. 3. Key HMBC and ^{1}H–^{1}H COSY correlations of compound **1**.*

3.2. Effect of M. procumbens extracts on intracellular lipid accumulation in 3T3-L1 cells

Four layers (MPM, MPH, MPD, and MPW) yielded from *M. procumbens* extracts were examined the cytotoxic effect on 3T3-L1 preadipocytes, which treated with 25 or 50 μg/mL of samples for 48 h, and cell viability was measured by CCK-8 assay. As shown in Fig. 2A, 50 μg/mL of MPH caused severe cell death, while the others showed little to no cytotoxic effect on 3T3-L1 preadipocytes. Next, 3T3-L1 cells were treated with 25 or 50 μg/mL of samples, and lipid accumulation of cells was measured using Oil Red O staining. As shown in Fig. 2B and C, samples exerted differential inhibitory effects on the inhibition of lipid accumulation in 3T3-L1 cells. Among these fractions, MPD showed the best activity in blocking lipid accumulation and had no obvious cytotoxic effect in 3T3-L1 cells.

3.3. Structural elucidation of the isolated compounds

Compound **1** was obtained as a colorless syrup. Its molecular formula, $C_{28}H_{40}O_{12}$, was established on the basis of the quasimolecular ion peak at *m/z* 591.2419 $[M + Na]^+$ (calcd. for $C_{28}H_{40}O_{12}Na$, 591.2412) in the HRESIMS. The IR and UV spectra displayed absorption bands for hydroxyl (3414 cm^{-1}), carbonyl (1731 cm^{-1}) and aromatic ester groups (1731 cm^{-1} and 273 nm). The ^{1}H-NMR spectrum (Table 1) of **1** exhibited signals for one triplet methyl at δ_H 0.92 (J = 7.0 Hz); one singlet methyl at δ_H 1.95; eight olefinic protons at 5.16 (ddd, J = 10.5, 1.5, 1.0 Hz), 5.29 (ddd, J = 17.0, 1.5, 1.0 Hz), 5.92 (ddd, J = 17.5, 10.5, 7.0 Hz), 7.49 (2H, m), 7.63 (1H, m), and 8.02 (2H, m). The ^{13}C-NMR (Table 2) spectrum showed 28 signals and when combined with the DEPT experiment showed that compound **1** contains a benzoate group (δ_C 166.1, 133.0, 129.7, 129.3, 129.3, 128.2, and 128.2), one acetoxy group (δ_C 19.2, and 170.3), two anomeric carbons (δ_C 101.9 and 103.8), eight oxygenated methine (δ_C 81.7, 76.1, 75.9, 73.4, 72.9, 72.1, 69.8, and 69.3), two oxygenated methylene (δ_C 67.5 and 65.5), one methyl (δ_C 13.0), two olefinic carbons (δ_C 115.0, and 139.3), and four sp^3 methylene carbons (δ_C 22.3, 24.2, 31.6, and 34.4). Two characteristic anomeric signals [δ_H 4.31 (d, J = 7.5 Hz), δ_C 101.9; 4.57 (d, J = 7.5 Hz), δ_C 103.8],

together with nine oxygenated carbons, indicated that compound **1** possesses a disaccharide moiety. Furthermore, detailed analyses of the ^{1}H and ^{13}C NMR spectroscopic data with the aid of $^{1}H-^{1}H$ COSY and HMBC correlation (Fig. 3) suggested that the disaccharide moiety should be as primeverose, including a glucopyranosyl group [δ_C 101.9 (C-1), 72.1 (C-2), 75.9 (C-3), 69.3 (C-4), 72.9 (C-5) and 67.5 (C-6)] and a xylopyranosyl group [δ_C 103.8 (C-1′), 73.4 (C-2′), 76.1 (C-3′), 69.8 (C-4′) and 65.5 (C-5′)] [16,17]. Moreover, the configurations of H-1 and H-1′ were assigned to be β-forms by the coupling constant (glu: J = 7.5 Hz and xyl: J = 7.5 Hz) and comparison of ^{13}C data with literature [17,18]. The $^{1}H-^{1}H$ COSY correlations of H-1″/H-2″/H-3″/H-4″/H-5″/H-6″/H-7″/H-8″ and H-1‴/H-2‴/H-3‴/H-4‴/H-5‴/H-6‴/H-7‴, in addition to the key HMBC correlations of H-3 (δ_H 5.36)/δ_C 166.1 and H-1 (δ_H 4.57) with δ_C 81.7 (C-3″), suggested that oct-1-en-3-ol was attached to C-1 and that benzoic acid was located at C-3. The acetoxy group was linked at C-4 by the HMBC correlation of H-4 (δ_H 5.12) with δ_C 170.3. Compound **1** was hydrolyzed with 2 N methanolic HCl to afford the algycone and sugar moieties. The aglycone was purified by HPLC and the stereochemistry of oct-1-en-3-ol group (matsutake alcohol) was identified as *R*-orientation by specific rotation $[\alpha]_D^{25}$ -4.3 (*c* 0.6, $CHCl_3$) and NMR data [15]. On the other hand, the sugar moieties were proven to be D-glucopyranose and D-xylopyranose based on GC analysis. Therefore, the structure of compound **1** was fully established as 1-(*R*)-oct-1-en-3-yl-3-*O*-benzoyl-4-*O*-acetyl-β-D-primeveroside and named mesonoside A.

Compound **2** was obtained as a colorless syrup and possessed a molecular formula of $C_{30}H_{42}O_{13}$ by its sodiated quasimolecular ion at *m/z* 633.2504 $[M + Na]^+$ (calcd. for $C_{30}H_{42}O_{13}Na$, 633.2518) in HRESIMS. The IR and UV spectra displayed absorption bands for the hydroxyl, carbonyl and aromatic ester groups. The ^{1}H and ^{13}C NMR data (Tables 1 and 2) were very similar to those of **1** along with the same substitution pattern, except for the presence of an extra acetyl group signal (δ_H 2.15 and δ_C 170.6, 19.9). Based on analysis of the HMBC experiment, the correlation between δ_H 4.71 (H-2′) and the carbonyl carbon (δ_C 170.6) suggested assignment of an acetyl group at C-2'. Consequently, **2** was deduced to be 1-(*R*)-oct-1-en-3-yl-3-*O*-benzoyl-4,2′-*O*-diacetyl-β-D-primeveroside and named mesonoside B.

The molecular formulas of compounds **3** and **4** were established as $C_{30}H_{42}O_{13}$ by quasimolecular ion peaks at *m/z* 633.2501 and 633.2500 $[M + Na]^+$ in the HRESIMS experiments, respectively, the same as those of **2**. Similar to those of **2**, both of the ^{1}H and ^{13}C NMR spectroscopic data (Tables 1 and 2) showed that compounds **3** and **4** possessed similar moieties, including primeverose, a benzoyl group, two acetyl groups, and a 1-(*R*)-oct-1-en-3-yl group. In **3**, the positions of the acetyl groups were determined at C-2' (δ_C 71.9) and C-3' (δ_C 75.3) by the HMBC correlations of H-2' (δ_H 4.72)/δ_C 167.0 and H-3' (δ_H 4.79)/δ_C 170.7. In **4**, two acetyl groups were assigned at C-4 and C-3′ based on the HMBC correlations of H-4 (δ_H 5.11)/δ_C 170.2 and H-3' (δ_H 4.89)/δ_C 171.2. On the basis of the above evidence, compounds **3** and **4** were identified as 1-(*R*)-oct-1-en-3-yl-3-*O*-benzoyl-2′,3′-*O*-diacetyl-β-D-primeveroside (mesonoside C) and 1-(*R*)-oct-1-en-3-yl-3-*O*-benzoyl-4,3′-*O*-diacetyl-β-D-primeveroside (mesonoside D), respectively.

Compound **5** has a quasimolecular ion peak at *m/z* 633.2507 $[M + Na]^+$, consistent with the molecular formula $C_{30}H_{42}O_{13}$, from analysis of its HRESIMS. The NMR data (Tables 1 and 2) were very similar to those of **4**, except for the proton resonance at δ_H 4.89 (H-3′) in **4** was shifed upfield to δ_H 3.57 in **5**, while the proton of H-4′ in **4** downfield to δ_H 4.71 in **5**. The findings indicated the acetyl group was shifted from C-3′ in **4** to C-4′ in **5**, and that was further confirmed by the HMBC correlation of H-4′/δ_C 170.8. Taken together, the above evidence determined that the structure of mesonoside E (**5**) was 1-(*R*)-oct-1-en-3-yl-3-*O*-benzoyl-4,4′-*O*-diacetyl-β-D-primeveroside.

Compound **6** was obtained as a colorless syrup and possessed a molecular formula of $C_{30}H_{42}O_{13}$ by its sodiated quasimolecular ion peak at *m/z* 675.2639 $[M + Na]^+$ (calcd. for $C_{30}H_{42}O_{13}Na$, 675.2623) in the HRESIMS. The ^{1}H and ^{13}C-NMR spectra (Tables 1 and 2) of **6** exhibited the presence of three acetyl groups (δ_H 1.90, 1.91, 2.12; δ_C 169.5, 169.7, 170.6, 19.1, 19.2, 19.8), a benzoate group (δ_C 165.7, 129.0, 129.3 × 2, 128.2 × 2, 133.3), two anomeric signals [δ_H 4.76 (d, J = 7.8 Hz), δ_C 99.5, glu-1; 4.41 (d, J = 7.8 Hz), 101.3, xyl-1], and a 1-oct-1-en-3-yl group [characteristic signals of one triplet methyl at δ_H 0.89 (J = 6.6 Hz) and 5.12 (ddd, J = 17.4, 1.5, 1.0 Hz), 5.24 (ddd, J = 10.8, 1.5, 1.0 Hz), 5.85 (ddd, J = 17.0, 10.5, 7.0 Hz), and 4.10 (ddd, J = 6.0, 6.5, 12.5 Hz)]. The ^{1}H and ^{13}C NMR data (Tables 1 and 2) were very similar to those of **2**, except for the addition of an acetyl group (δ_H 2.07; δ_C 170.0, 19.6). Furthermore,

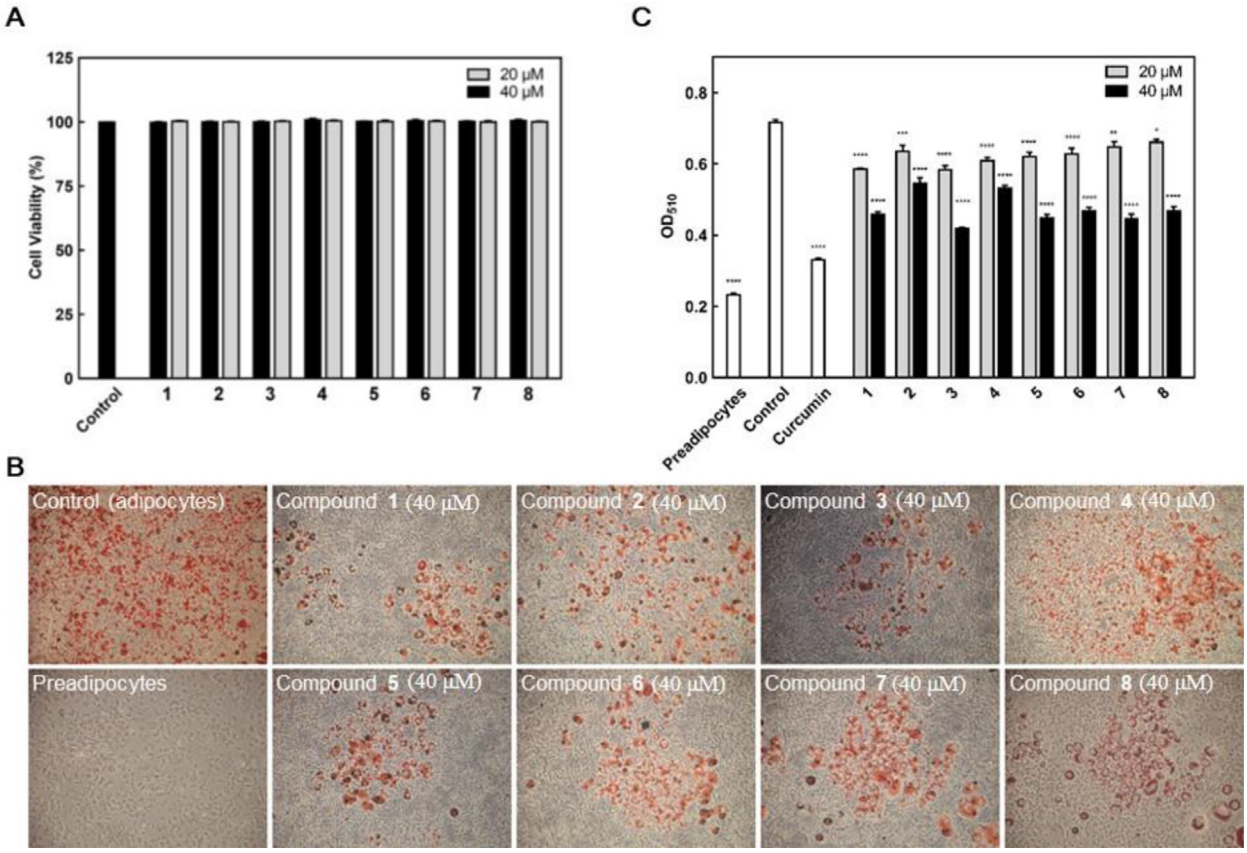

*Fig. 4. Effects of compounds **1**−**8** on the cytotoxicity and adipogenesis of 3T3-L1 cells. (A) Cell viability of compounds **1**−**8**. Lipid accumulation was visualized (B) and quantified (C) by Oil Red O staining. Curcumin (Cur, 15 μM) was the positive control. Values are presented as the mean ± SD (n = 3). Values with different letters indicate significant differences as determined by Dunnett's method. *p < 0.05, **p < 0.01, ***p < 0.001, ****p < 0.0001 relative to the control group.*

the acetyl group was assigned at C-2 (δ_C 71.9) by HMBC correlation between H-2′ [δ_H 0.89, dd (J = 9.5, 8.0 Hz)] and δ_C 170.0. Consequently, **6** was deduced to be 1-(*R*)-oct-1-en-3-yl-3-*O*-benzoyl-2,4,2′-*O*-triacetyl-β-D-primeveroside and named mesonoside F.

Similar to **6**, compounds **7** and **8** also possessed similar 1D and 2D NMR, UV, IR, and HRESIMS spectra. The HRESIMS of **7** and **8** suggested a molecular formula of $C_{30}H_{42}O_{13}$ based on its sodiated quasimolecular ion peak at *m/z* 675.2631 in **7** and 675.2603 in **8** ($[M + Na]^+$, calcd. for $C_{32}H_{44}O_{14}Na$, 675.2623). The IR spectra displayed absorption bands for hydroxyl, carbonyl, and aromatic groups, and the UV spectra showed absorption maxima at 273 and 229 nm. The ^1H and ^{13}C-NMR spectroscopic data of compounds **7** and **8** (Tables 1 and 2) suggested that their structures were similar to **6** which belong to 1-(*R*)-oct-1-en-3-yl-3-*O*-benzoyl primeverose derivatives with three acetyl groups. Detailed analysis of the HMBC correlations revealed that three acetyl groups were located at C-4, C-2′ and C-3′ in **7** but located at C-4, C-2′ and C-4′ in **8**. Therefore, mesonosides G (**7**) and H (**8**) were identified as 1-(*R*)-oct-1-en-3-yl-3-*O*-benzoyl-4,2′,3′-*O*-triacetyl-β-D-primeveroside and 1-(*R*)-oct-1-en-3-yl-3-*O*-benzoyl-4,2′,4′-*O*-triacetyl-β-D-primeveroside, respectively.

3.4. Identification of the isolated compounds from MPD on HPLC fingerprint profile

We studied the HPLC fingerprints of the bioactive MPD layer from *M. procumbens* and analyzed them under the following conditions: The mobile phase consisted of water containing 0.1% phosphoric acid

and ACN using a gradient program of 5−45% ACN from 0 to 25 min, 45-45% ACN from 20 to 40 min, 45−80% ACN from 40 to 55 min and 80−100% ACN from 55 to 65 min; separation was achieved on a Cosmosil 5C_{18}-AR-II column (5 μm, 250 mm × 4.6 mm i.d.) with a flow rate of 1.0 mL/min at 35 °C; real-time UV absorption was detected at 254 nm. Seven isolated compounds were successfully recognized in the HPLC fingerprints of MPD layer, and their retention times (RTs) were 33.82 min (**1**), 42.97 min (**2**), 44.24 min (**3**), 45.52 min (**4**), 46.11 min (**5**), 49.76 min (**7**), and 50.23 min (**8**), respectively (Supplementary Fig. S1). Due to the most yielded amounts together with high resolution and well separation around its corresponding peak in HPLC fingerprints of MPD layer, **1** could be served as the target compound for the quality control of *M. procumbens*.

3.5. Effects of compounds 1−8 on intracellular lipid accumulation in 3T3-L1 cells

The cell survival assay showed that all compounds (**1**−**8**) exhibited little or no cytotoxic effects in 3T3-L1 preadipocytes at 20 or 40 μM (Fig. 4A). We next examined the effects of compounds **1**−**8** on intracellular lipid accumulation in 3T3-L1 adipocytes.

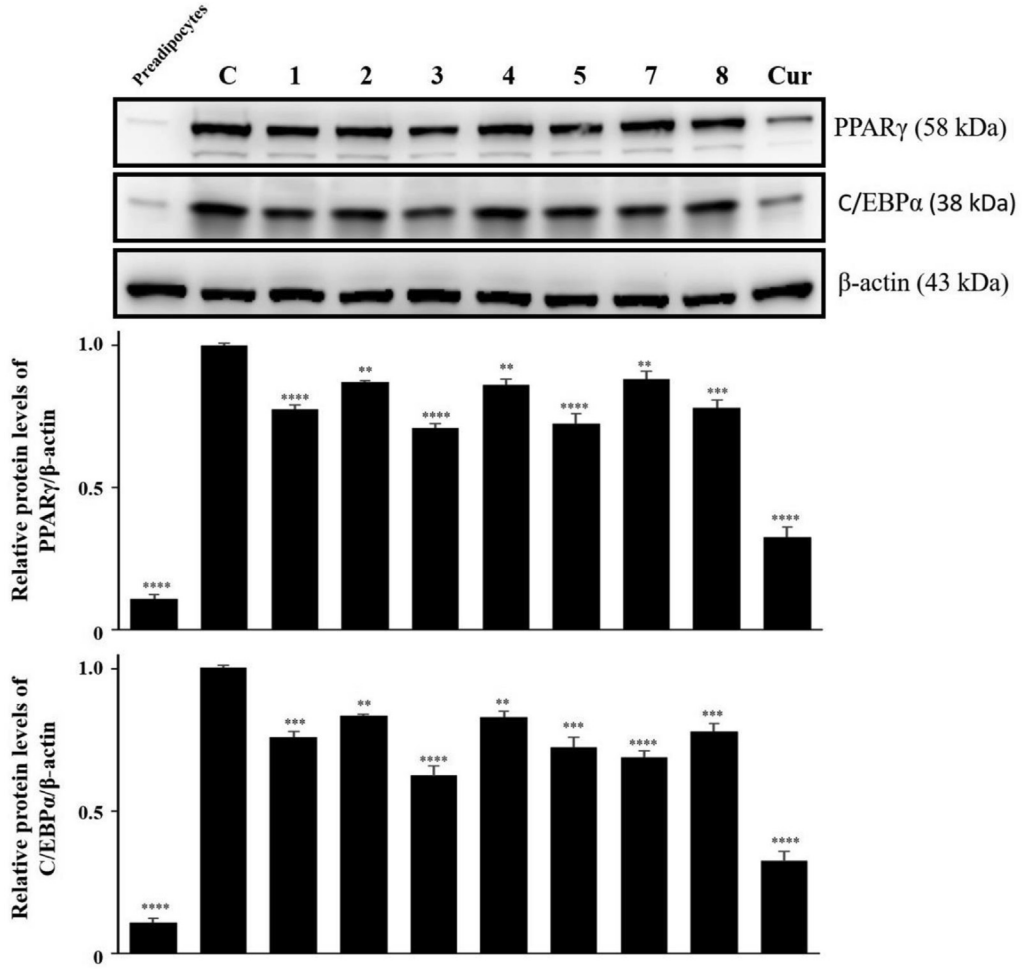

*Fig. 5. Compounds **1**−**5**, **7**, and **8** inhibited the expression of PPARγ and C/EBPα in 3T3-L1 cells. 3T3-L1 cells (1.5 × 10^5 cells/6-cm dish) were treated with compounds **1**−**5**, **7**, and **8** (40 μM) for 8 d. Curcumin (Cur, 15 μM) was the positive control. The total protein of each group was extracted, and the expression of PPARγ and C/EBPα was determined by western blotting. The relative levels of PPARγ and C/EBPα were quantified by normalizing with the β-actin levels. Values with different letters indicate significant differences as determined by Dunnett's method. *$p < 0.05$, **$p < 0.01$, ***$p < 0.001$, ****$p < 0.0001$ relative to the control group.*

The staining of lipid droplets with Oil Red O solution showed that compounds **1**–**8** inhibited lipid droplet accumulation from 8.2 to 18.7% at 20 μM and 24.3–42.0% at 40 μM in the adipocytes (Fig. 4B and C). Notably, compounds **1**–**8** all showed a significant decrease in lipid accumulation in a dose-dependent manner in 3T3-L1 cells. Among these isolates, compound **3** showed the most inhibition in 3T3-L1 cells.

3.6. Effect of the isolated compounds on key adipogenic gene regulators, PPARγ and C/EBPα protein levels, in 3T3-L1 cells

In mammalian cells, PPARγ and C/EBPα are the main regulators of adipogenesis and have been shown to have a broad overlap in their transcriptional targets [1]. To further investigate the underlying mechanism by which compounds **1**–**5**, **7**, and **8** attenuate lipid accumulation in 3T3-L1 cells, we examined the protein levels of critical regulators of adipogenesis, PPARγ and C/EBPα. After treatment with 40 μM of compounds **1**–**5**, **7**, and **8** for 8 d, total protein was extracted, and Western blot analysis was used to detect PPARγ and C/EBPα protein levels. As shown in Fig. 5, the PPARγ and C/EBPα levels were significantly reduced in cells treated with compounds **1**–**5**, **7**, and **8** compared to control cells. These results indicate that compounds **1**–**5**, **7**, and **8** may suppress lipid accumulation in 3T3-L1 cells by decreasing the protein levels of PPARγ and C/EBPα, critical adipogenic gene regulators. Notably, **3** exhibits the most inhibition of lipid accumulation, not only in 3T3-L1 cells, but also in the protein levels of PPARγ and C/EBPα.

Our results are consistent with a recent study that eugenol diglycosides inhibited lipid droplet accumulation in adipocytes by reducing the transcription levels of adipocyte marker genes (*Fabp4, PPARγ, C/EBPβ, Adipsin*, and *Adipoq*) [7]. Here, we demonstrated the anti-adipogenic bioactivity of *M. procumbens* and further isolation and identification of eight new primeverose derivatives (**1**–**8**) from a methanolic extract of *M. procumbens.* Furthermore, the anti-adipogenic effect of the isolated compounds (**1**–**5**, **7**, and **8**) may occur via the inhibition of PPARγ and C/EBPα protein levels. Our studies provide scientific evidence to support this plant serving to reduce the level of intracellular lipid droplet accumulation.

4. Conclusion

In the report, we have isolated and identified eight new primeverose derivatives from the methanolic extract of *M. procumbens*. Those isolates (**1**–**5**, **7**, and **8**), which possessed primeverose unit and substituted with benzoyl, acetyl, and oct-1-en-3-ol groups, showed the inhibitory effect on lipid accumulation in 3T3-L1 cells by suppressing expression the PPARγ and C/EBPα protein levels of the adipogenic transcription factors. The findings provide a potential therapeutic strategy to use primeverose derivatives the major components isolated from *M. procumbens* on the treatment of excessive adipogenesis in obesity.

Conflict of interest

The authors declare no conflicts of interest.

Acknowledgments

The authors gratefully acknowledge the support of the Ministry of Science and Technology of Taiwan (MOST 107-2320-B-077-003-MY3) for funding this work.

Appendix. Supplementary data

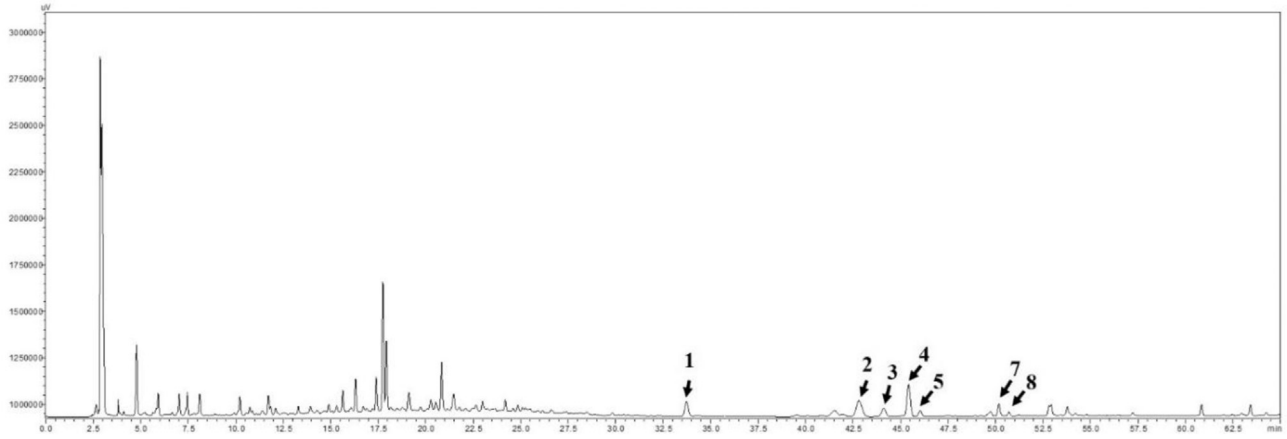

*Fig. S1 Identification of the active compounds **1**–**5**, **7**, and **8** in the HPLC fingerprint of the MPD layer.*

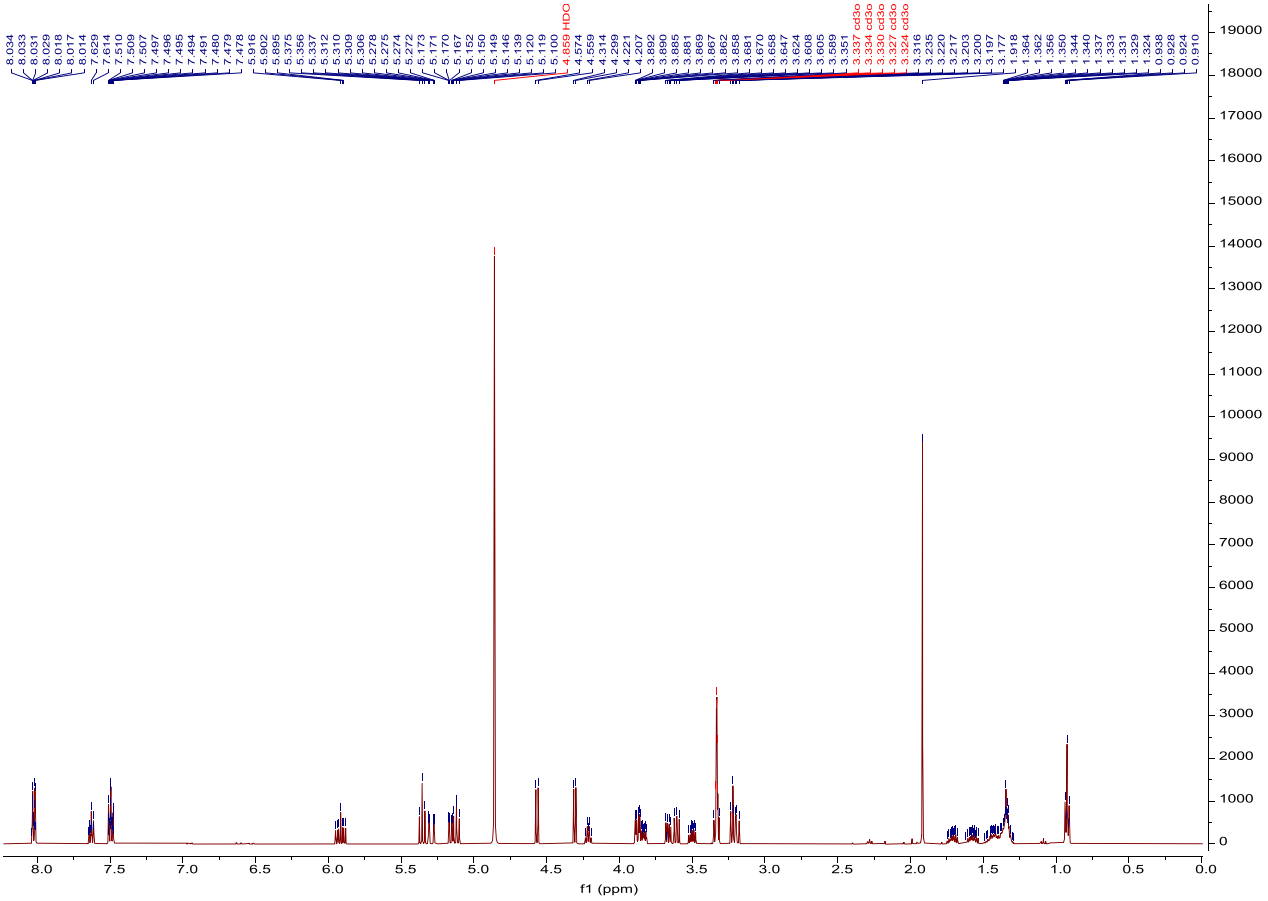

*Fig. S2 ^{1}H-NMR spectrum of mesonoside A (**1**) (500 MHz in methanol-d_4).*

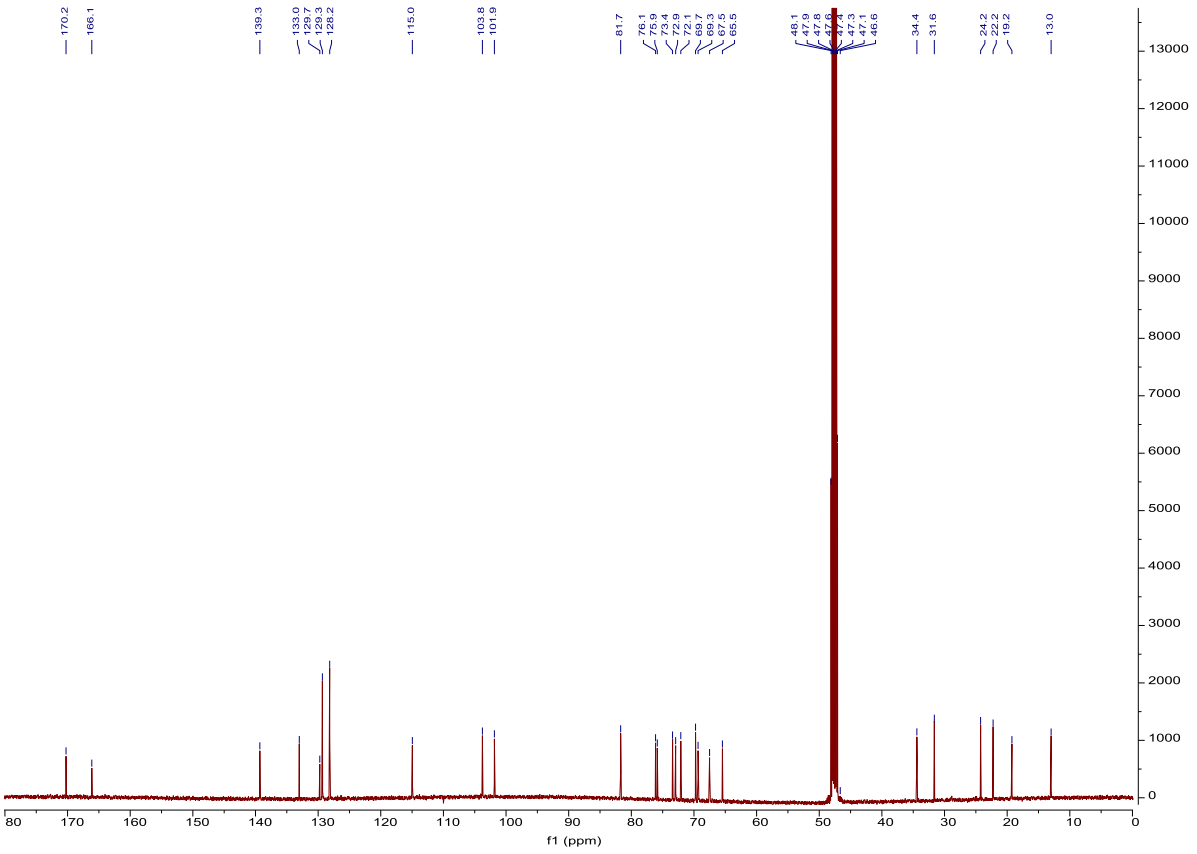

*Fig. S3 ^{13}C-NMR spectrum of mesonoside A (**1**) (125 MHz in methanol-d_4).*

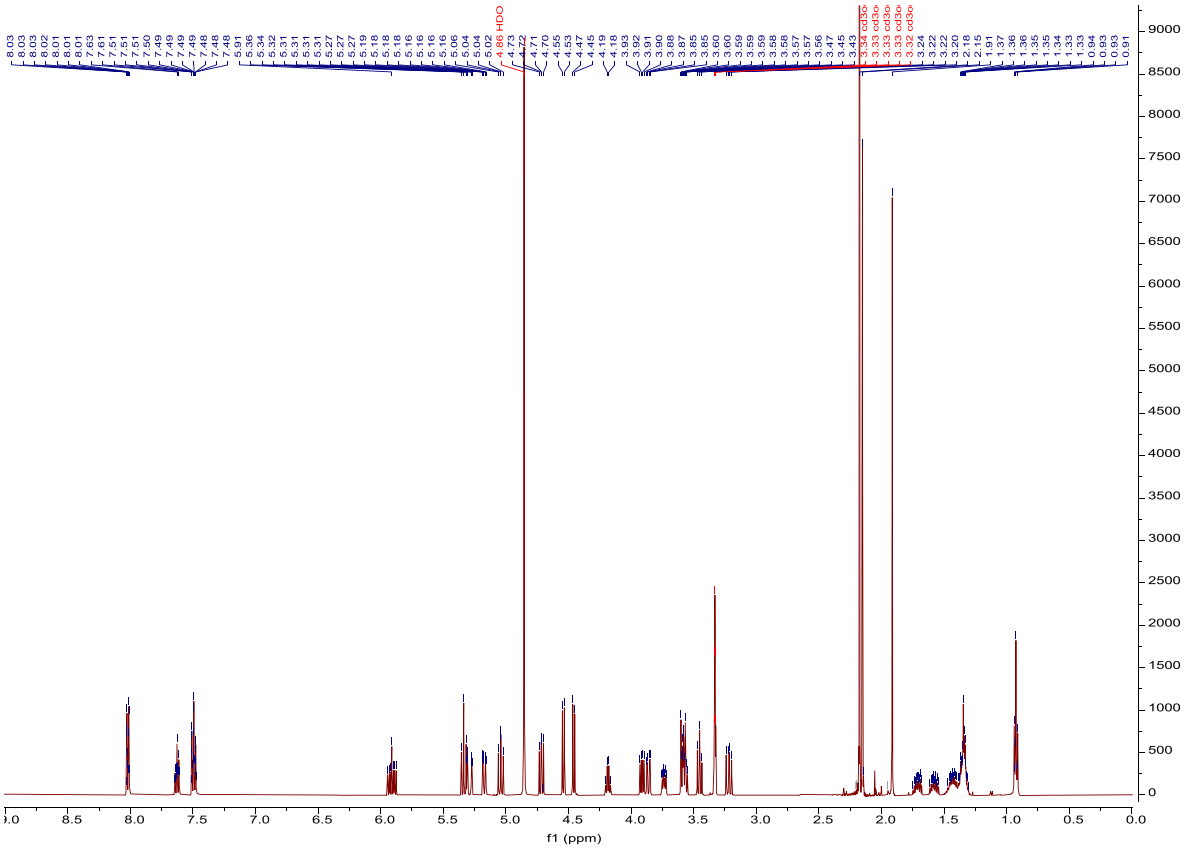

*Fig. S4 ^{1}H-NMR spectrum of mesonoside B (**2**) (500 MHz in methanol-d_4).*

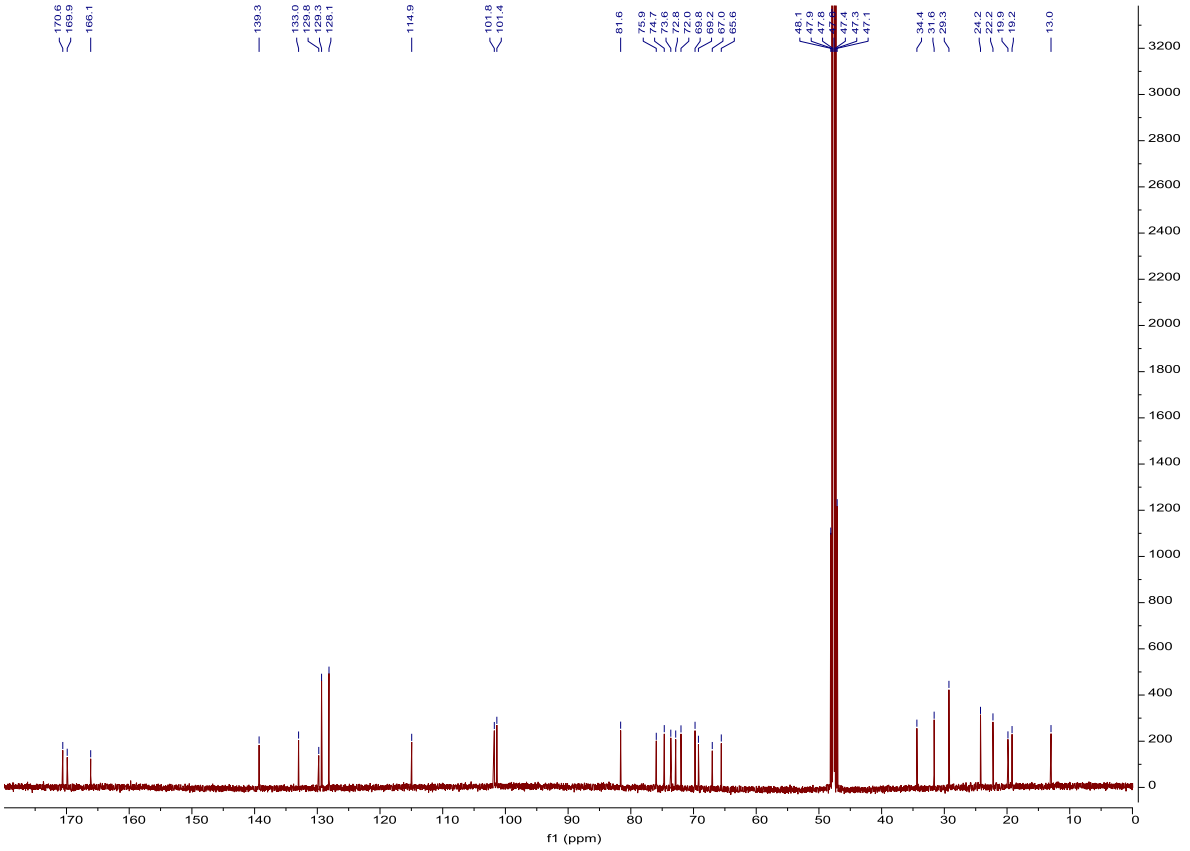

Fig. S5 ^{13}C-NMR spectrum of mesonoside B (2) (125 MHz in methanol-d_4).

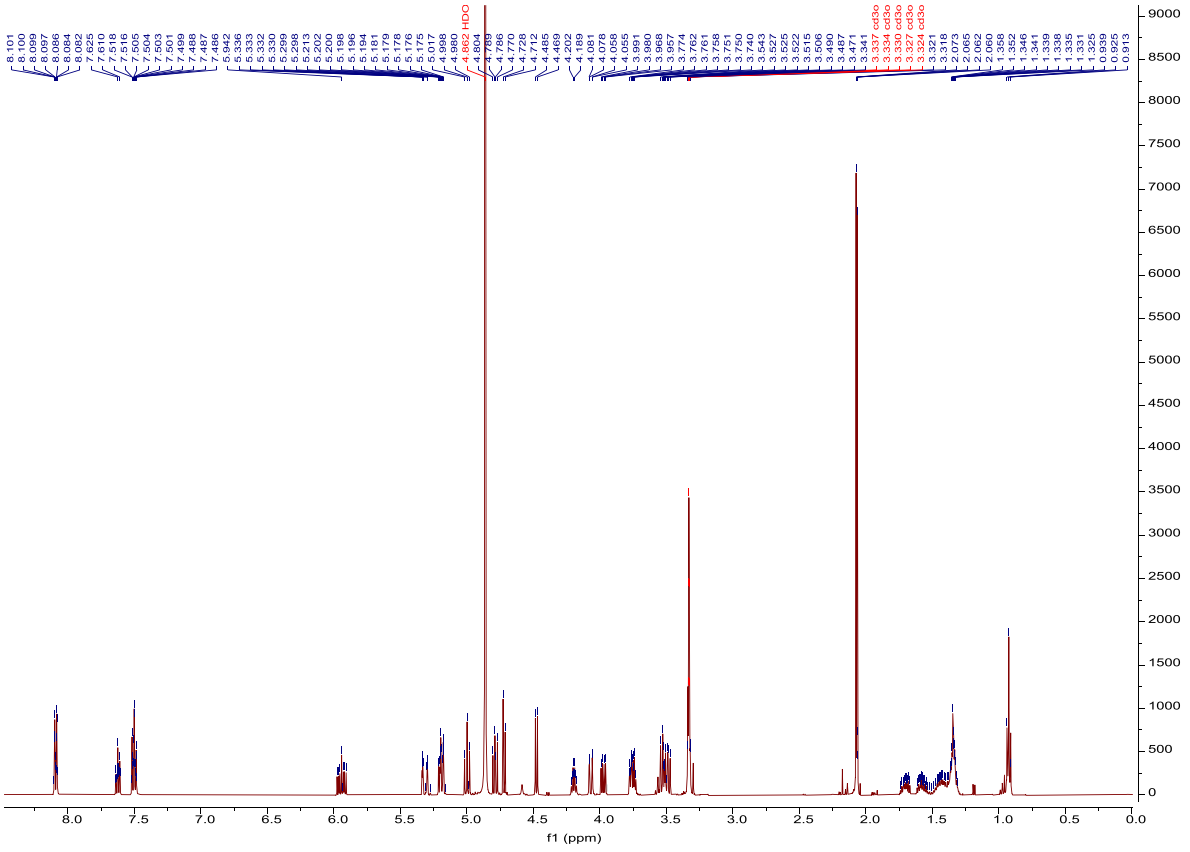

Fig. S6 ^{1}H-NMR spectrum of mesonoside C (3) (500 MHz in methanol-d_4).

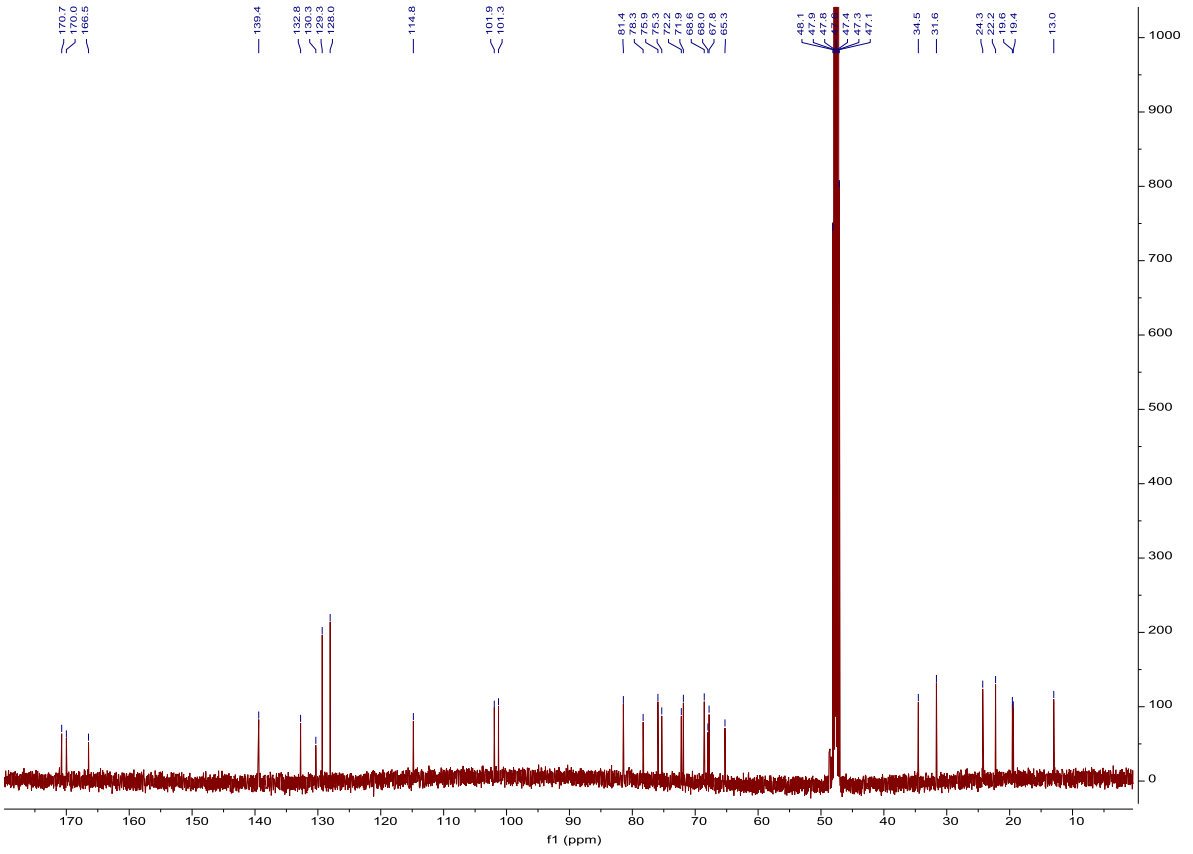

Fig. S7 ^{13}C-NMR spectrum of mesonoside C (3) (125 MHz in methanol-d_4).

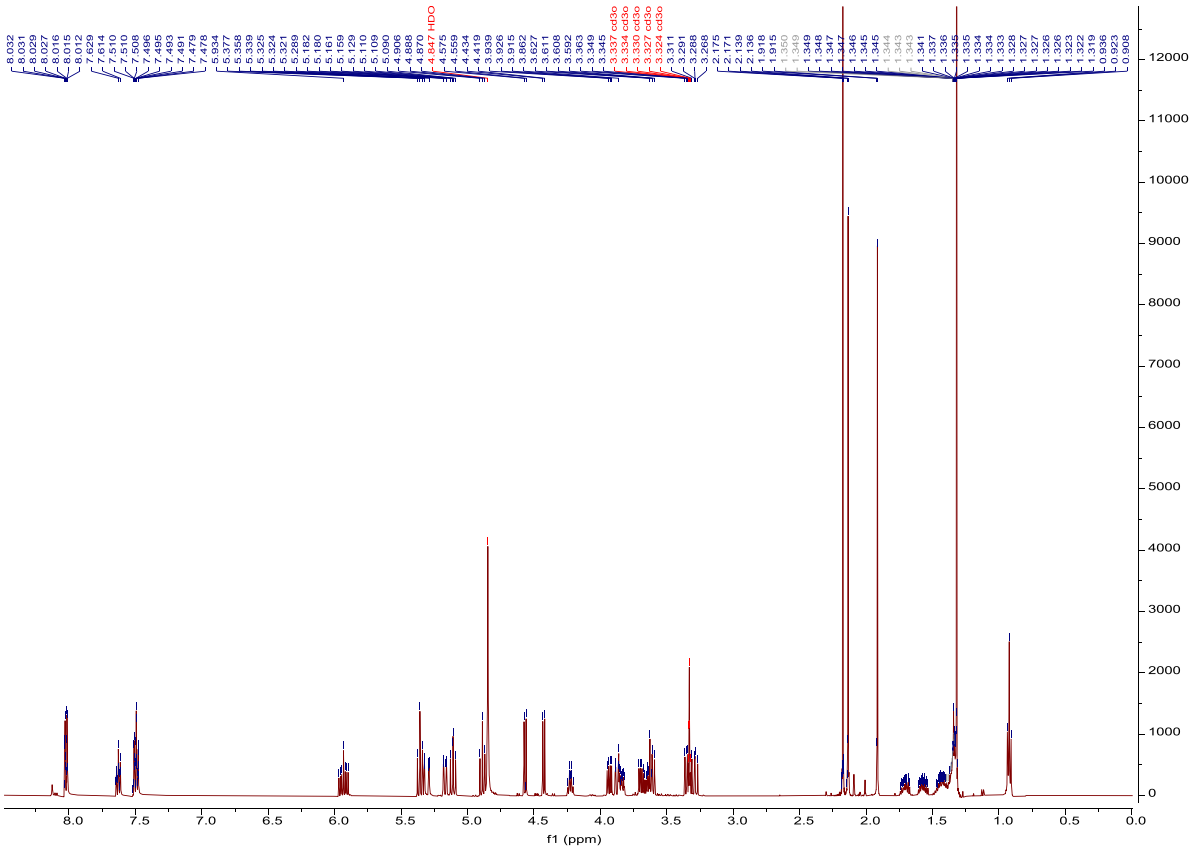

Fig. S8 ^{1}H-NMR spectrum of mesonoside D (4) (500 MHz in methanol-d_4).

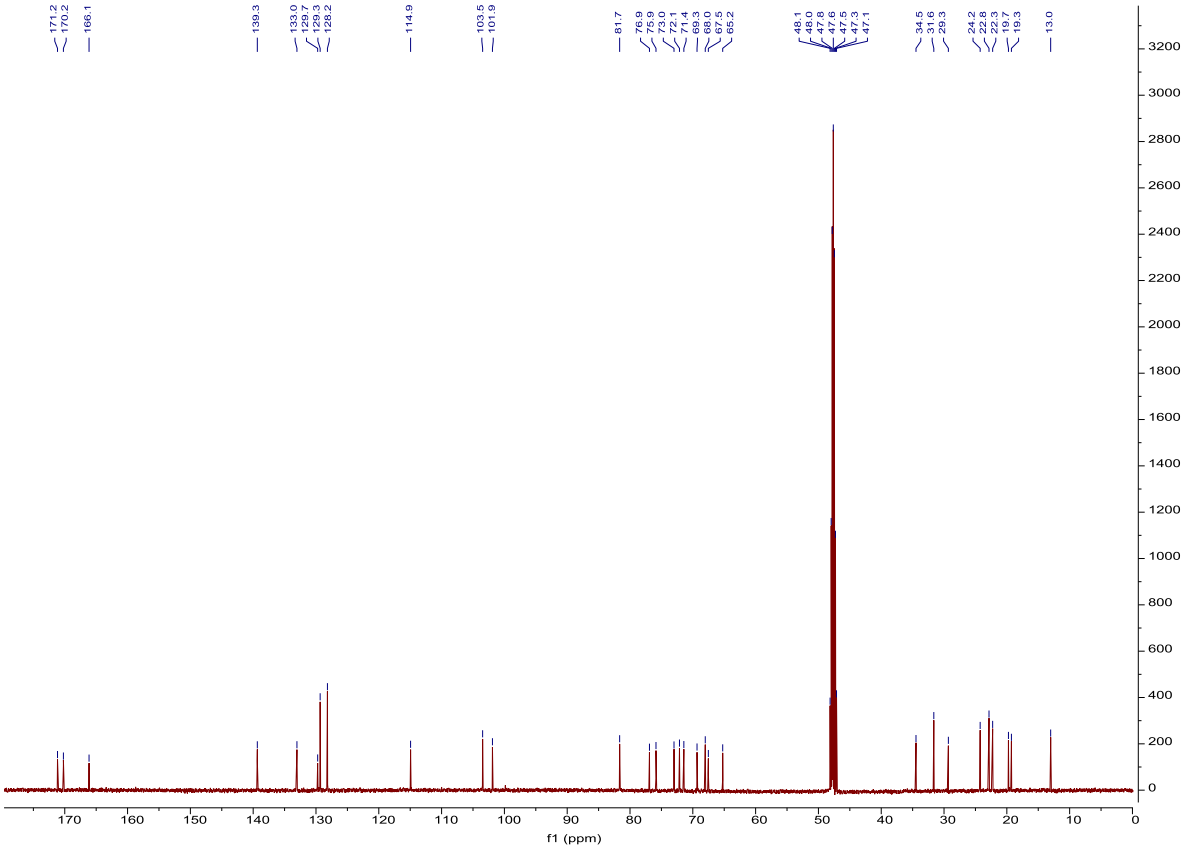

*Fig. S9 ^{13}C-NMR spectrum of mesonoside D (**4**) (125 MHz in methanol-d_4).*

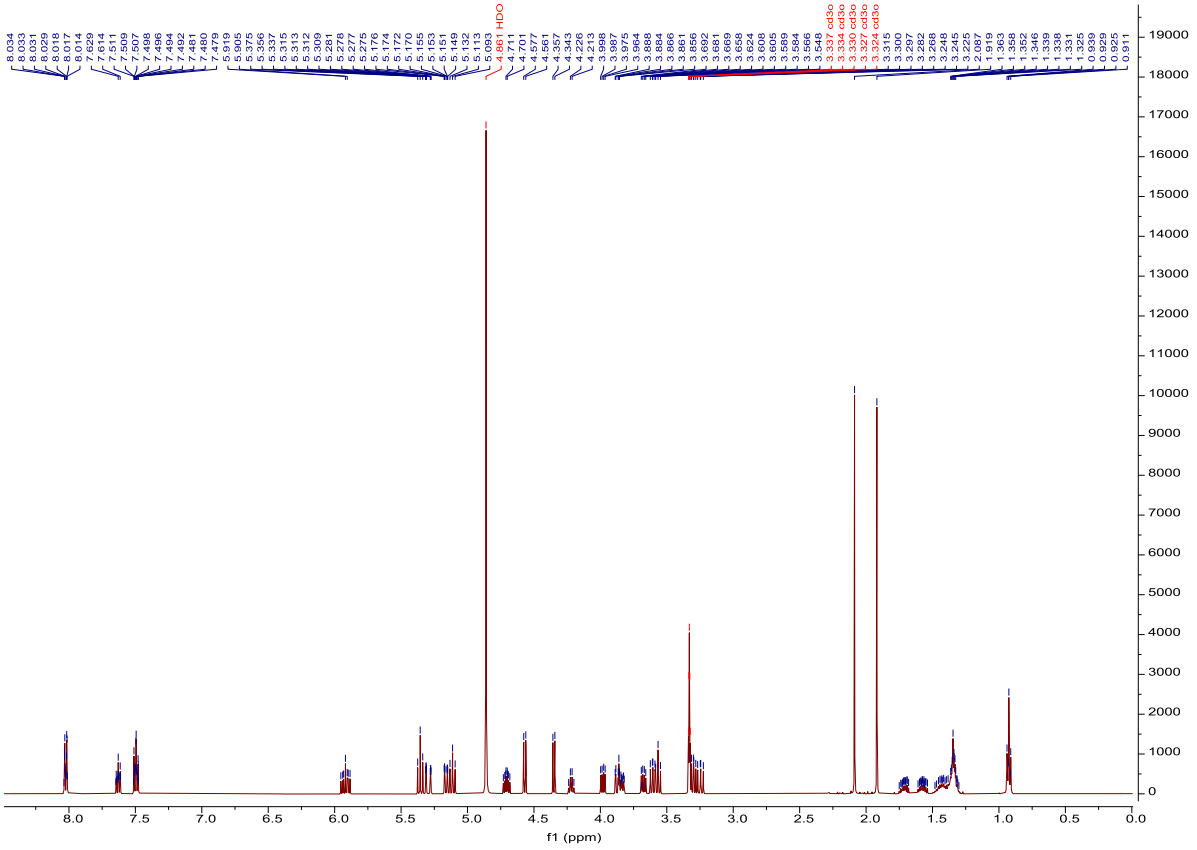

*Fig. S10 ^{1}H-NMR spectrum of mesonoside E (**5**) (500 MHz in methanol-d_4).*

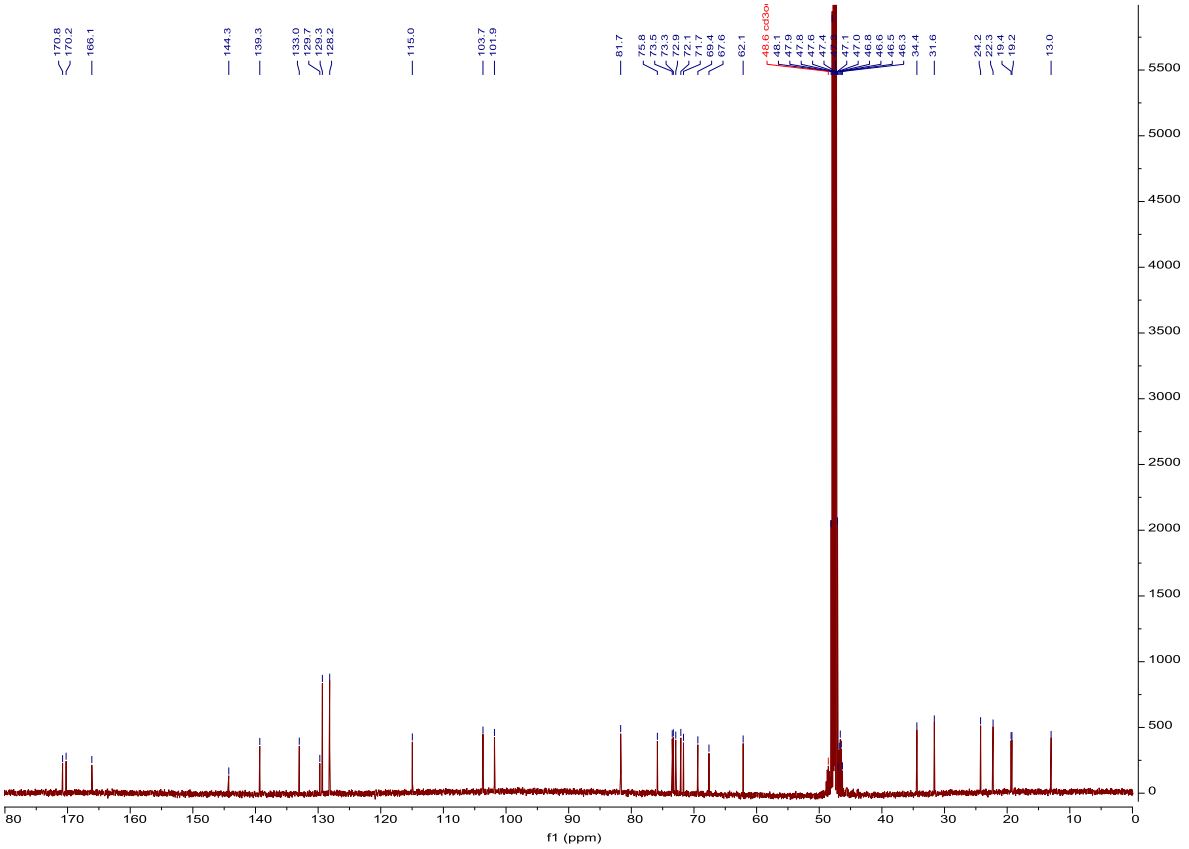

*Fig. S11 ^{13}C-NMR spectrum of mesonoside E (**5**) (125 MHz in methanol-d_4).*

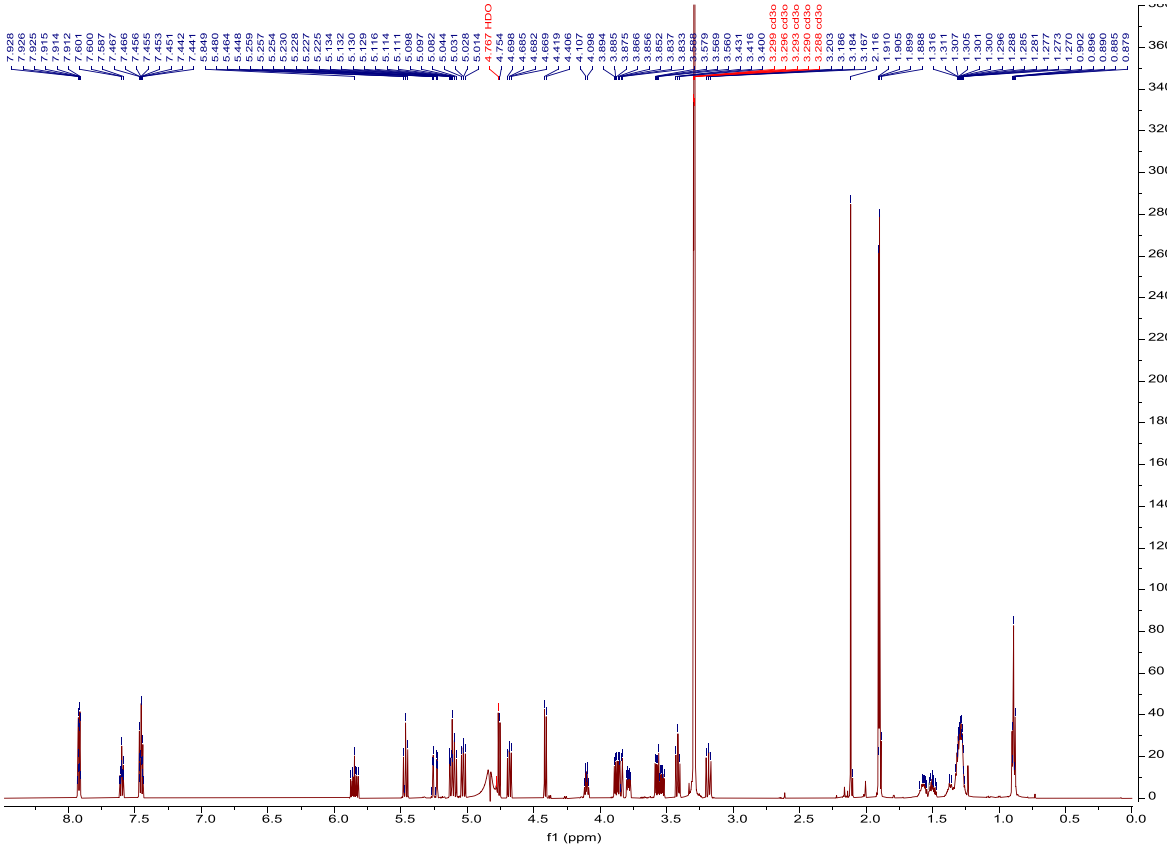

*Fig. S12 ^{1}H-NMR spectrum of mesonoside F (**6**) (600 MHz in methanol-d_4).*

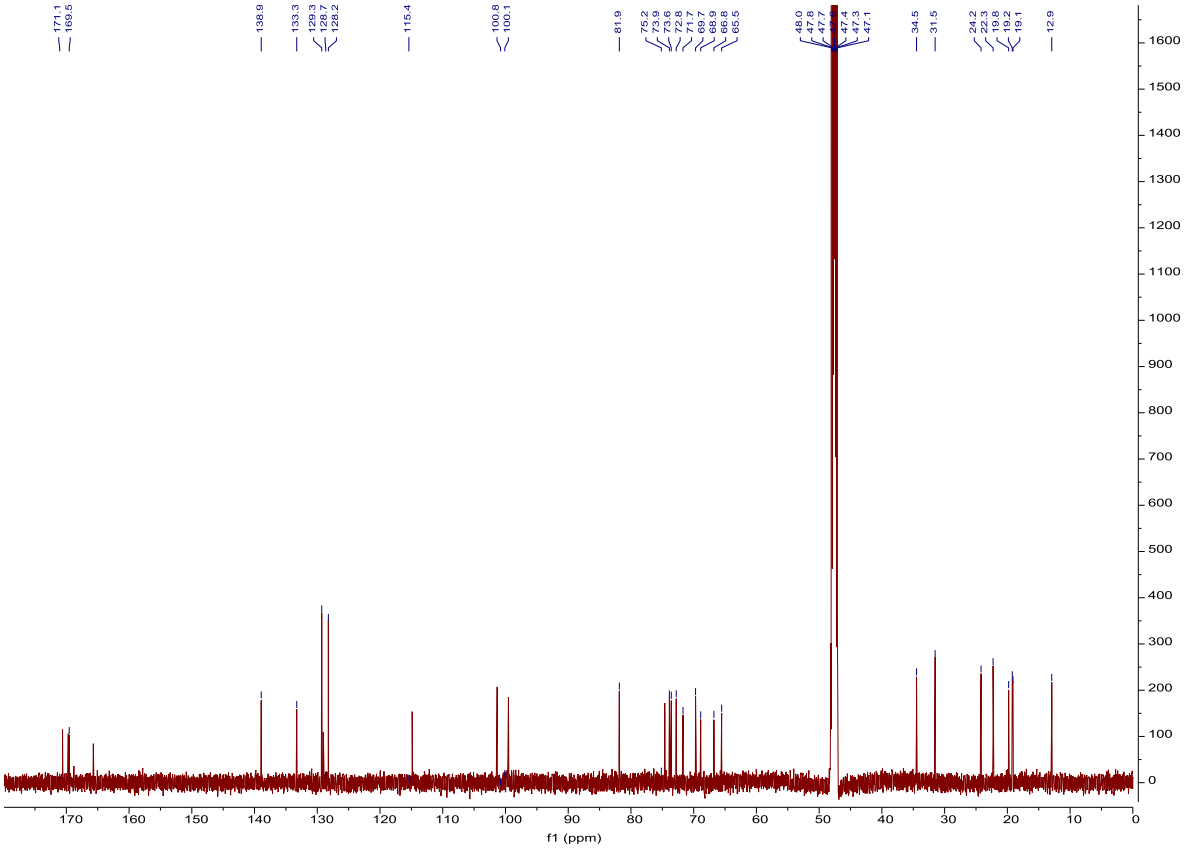

*Fig. S13 ^{13}C-NMR spectrum of mesonoside F (**6**) (150 MHz in methanol-d_4).*

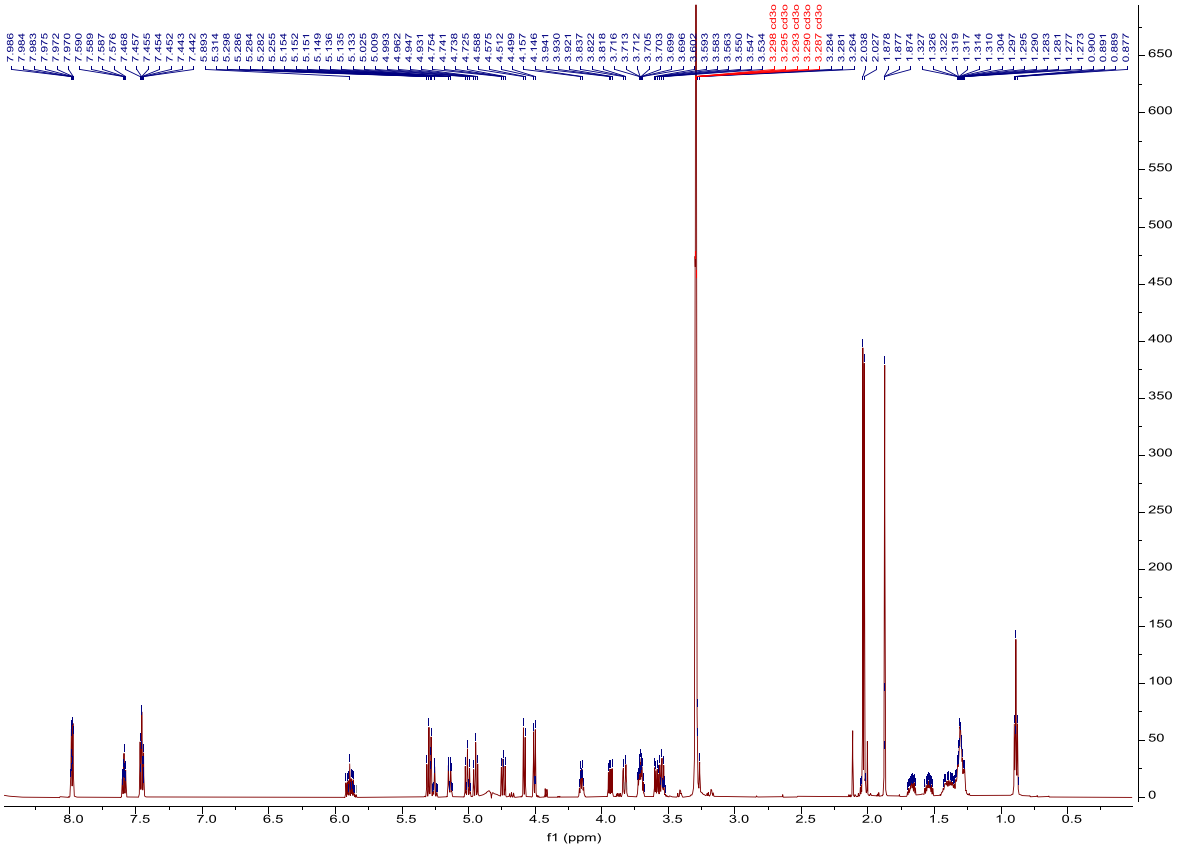

*Fig. S14 ^{1}H-NMR spectrum of mesonoside G (**7**) (600 MHz in methanol-d_4).*

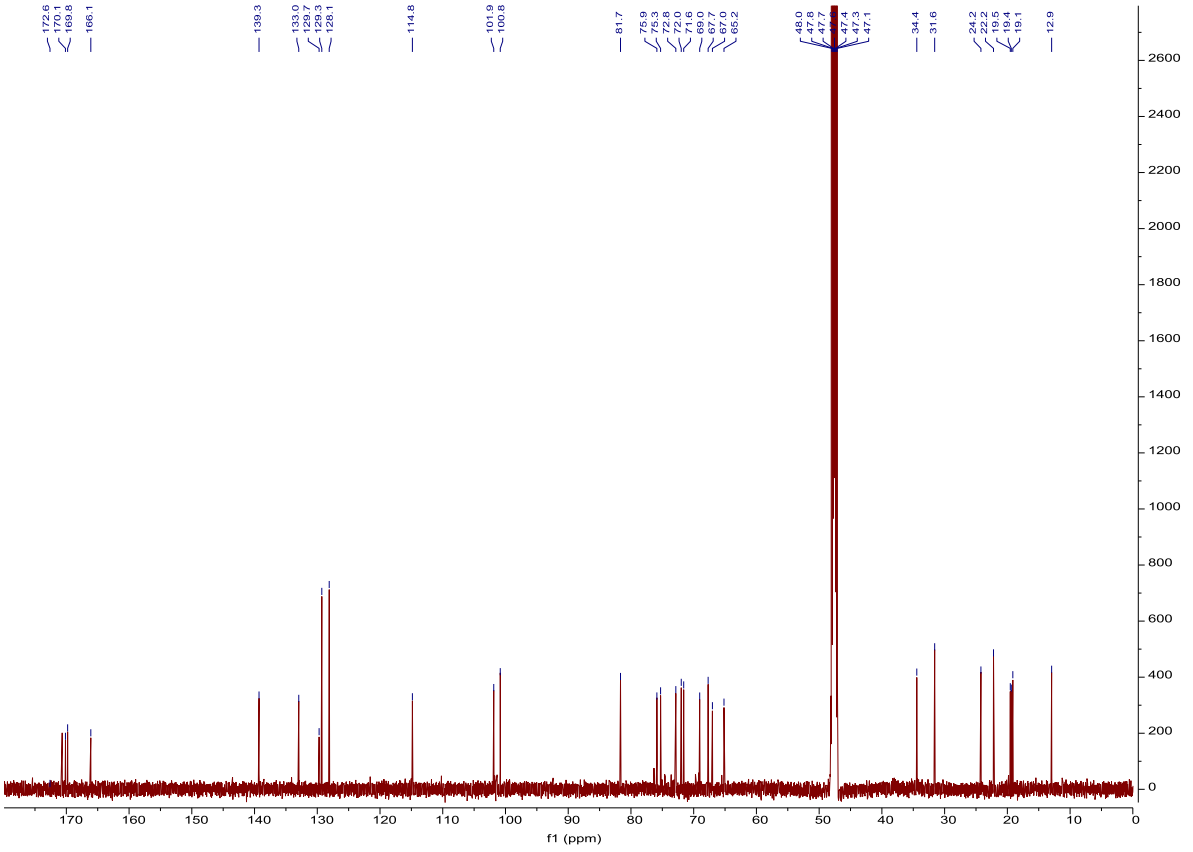

Fig. S15 ^{13}C-NMR spectrum of mesonoside G (7) (150 MHz in methanol-d_4).

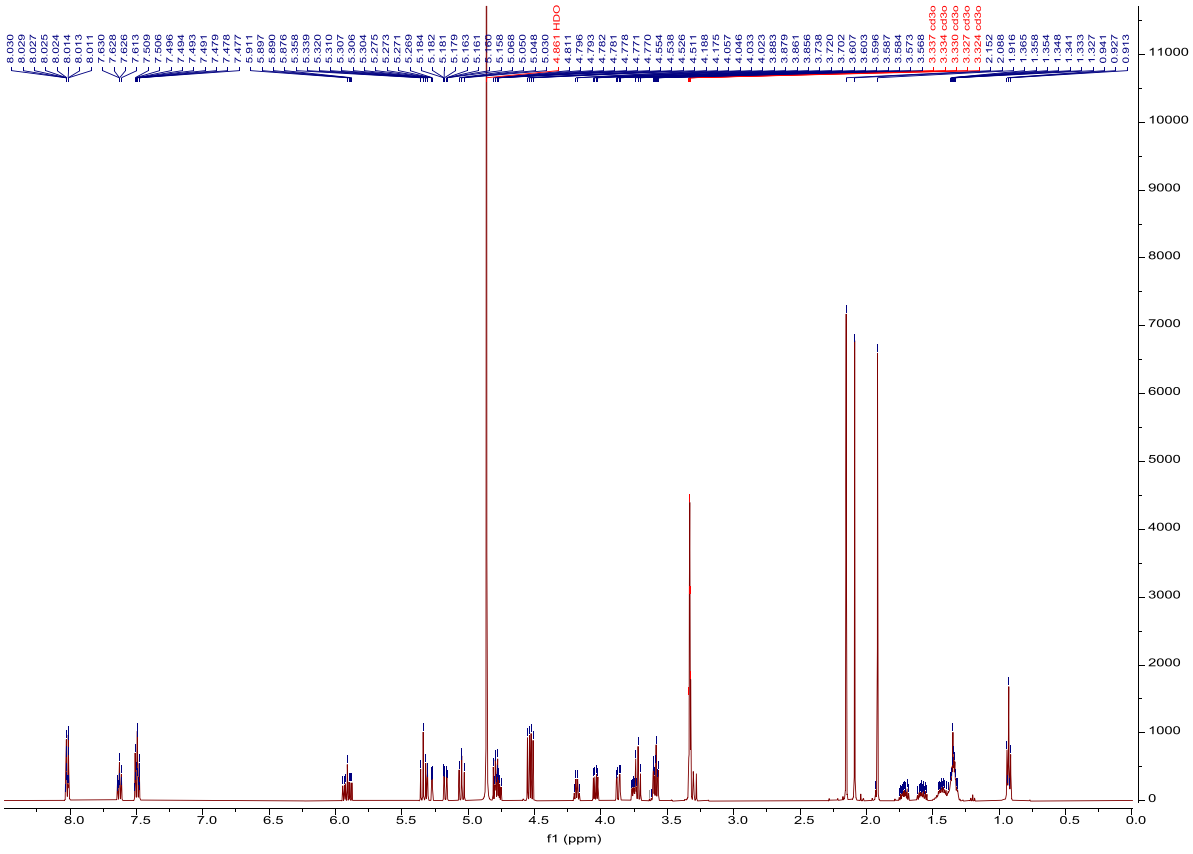

Fig. S16 ^{1}H-NMR spectrum of mesonoside H (8) (500 MHz in methanol-d_4).

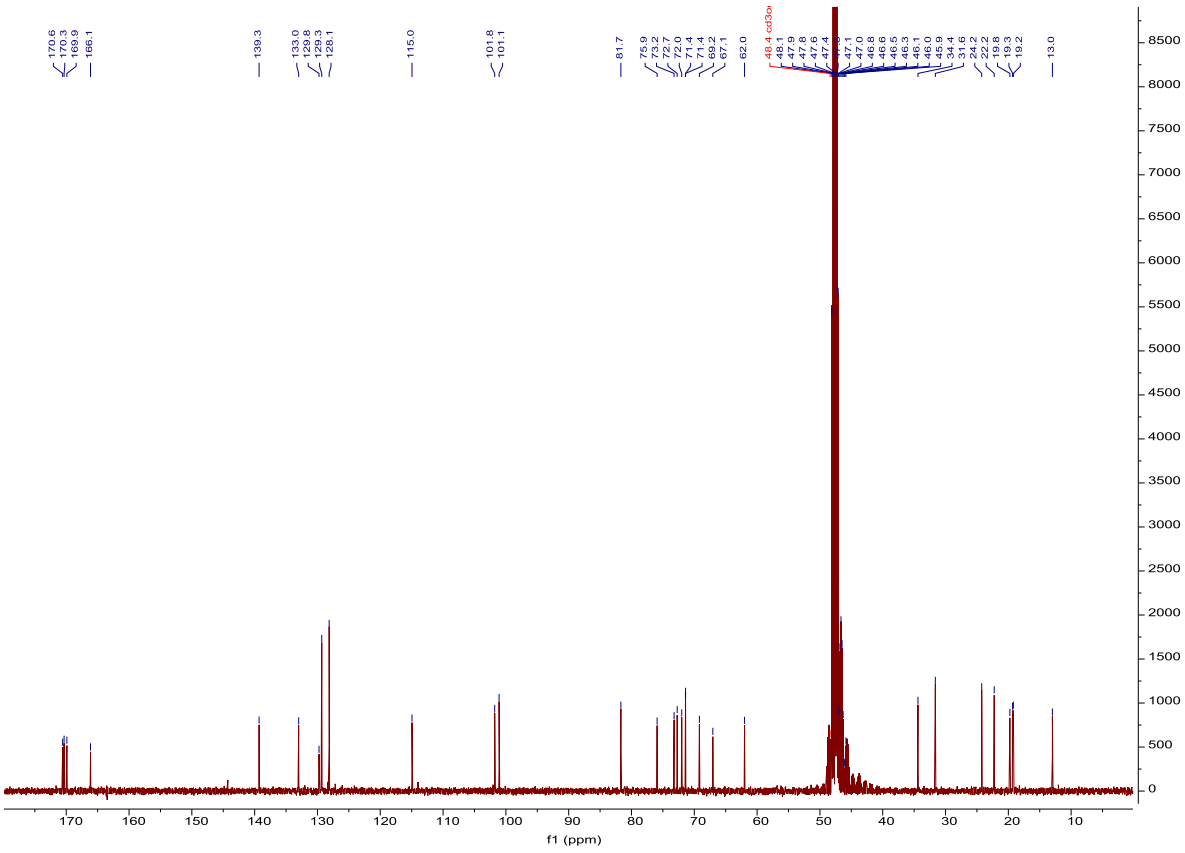

Fig. S17 ^{13}C-NMR spectrum of mesonoside H (8) (125 MHz in methanol-d_4).

References

[1] Formiguera X, Cantón A. Obesity: epidemiology and clinical aspects. Best Pract Res Clin Gastroenterol 2004;18:1125−46.

[2] Kopelman PG. Obesity as a medical problem. Nature 2000; 404:635−43.

[3] Furuyashiki T, Nagayasu H, Aoki Y, Bessho H, Hashimoto T, Kanazawa K, et al. Tea catechin suppresses adipocyte differentiation accompanied by down-regulation of PPARgamma2 and C/EBPalpha in 3T3-L1 cells. Biosci Biotechnol Biochem 2004;68:2353−9.

[4] Ghaben AL, Scherer PE. Adipogenesis and metabolic health. Nat Rev Mol Cell Biol 2019;20:242−58.

[5] Yeh WC, Cao Z, Classon M, McKnight SL. Cascade regulation of terminal adipocyte differentiation by three members of the C/EBP family of leucine zipper proteins. Genes Dev 1995;9:168−81.

[6] Fève B. Adipogenesis: cellular and molecular aspects. Best Pract Res Clin Endocrinol Metabol 2005;19:483−99.

[7] Baek SC, Nam KH, Yi SA, Jo MS, Lee KH, Lee YH, et al. Anti-adipogenic effect of β-carboline alkaloids from garlic (*Allium sativum*). Foods 2019;8:673−83.

[8] Yen GC, Yeh CT, Chen YJ. Protective effect of Mesona procumbens against tert- butyl hydroperoxide-induced acute hepatic damage in rats. J Agric Food Chem 2004;52:4121−7.

[9] Huang GJ, Liao JC, Chiu CS, Huang SS, Lin TH, Deng JS. Anti-inflammatory activities of aqueous extract of *Mesona procumbens* in experimental mice. J Sci Food Agric 2012;92: 1186−93.

[10] Yeh CT, Huang WH, Yen GC. Antihypertensive effects of Hsian-tsao and its active compound in spontaneously hypertensive rats. J Nutr Biochem 2009;20:866−75.

[11] Yen GC, Hung YL, Hsieh CL. Protective effect of extracts of *Mesona procumbens Hemsl*. on DNA damage in human lymphocytes exposed to hydrogen peroxide and UV irradiation. Food Chem Toxicol 2000;38:747−54.

[12] Yen GC, Duh PD, Hung YL. Contributions of major components to the antimutagenic effect of Hsian-Tsao (*Mesona procumbens Hemsl*.). J Agric Food Chem 2001;49:5000−4.

[13] Shyu MH, Kao TC, Yen GC. Hsian-Tsao (*Mesona procumbens Heml*.) prevents against rat liver fibrosis induced by CCl(4) via inhibition of hepatic stellate cells activation. Food Chem Toxicol 2008;46:3707−13.

[14] Yang M, Xu ZP, Xu CJ, Meng J, Ding GQ, Zhang XM, et al. Renal protective activity of hsian-tsao extracts in diabetic rats1 1this research was supported by the science found of Zhejiang Province (No. 2004C32082). Biomed Environ Sci 2008;21:222−7.

[15] Green H, Kehinde O. Sublines of mouse 3T3 cells that accumulate lipid. Cell 1974;1:113−6.

[16] Wojciechowicz T, Skrzypski M, Kołodziejski PA, Szczepankiewicz D, Pruszyńska-Oszmałek E, Kaczmarek P, et al. Obestatin stimulates differentiation and regulates lipolysis and leptin secretion in rat preadipocytes. Mol Med Rep 2015;12:8169−75.

[17] Feng J, Yi X, Huang W, Wang Y, He X. Novel triterpenoids and glycosides from durian exert pronounced anti-inflammatory activities. Food Chem 2018;241:215−21.

[18] Yamamura S, Ozawa K, Ohtani K, Kasai R, Yamasaki K. Antihistaminic flavones and aliphatic glycosides from *Mentha spicata*. Phytochemistry 1998;48:131−6.